IEEE Open Journal of the
Industrial Electronics Society

Received 16 June 2026; revised 20 July 2026; accepted 4 August 2026. Date of publication 7 August 2026;
date of current version 28 August 2026. The review of this article was arranged by Associate Editor Guanghui Wen.

Digital Object Identifier 10.1109/OJIES.2026.3721426

Practical Prescribed-Time Parameter Estimation for Underactuated Uncrewed Surface Vessel Based on DREM Method and LOS Control

JAWHAR GHOMMAM [1], MAAROUF SAAD [2] (Senior Member, IEEE), IBRAHIM AL-NAIMI [1], MAJDI MANSOURI [1], AND FAISAL MNIF [1] (Senior Member, IEEE)

[1]Sultan Qaboos University, Seeb 123, Oman
[2]Département de Génie Électrique, École de Technologie Supérieure, Montréal, QC H3C 1K3, Canada

CORRESPONDING AUTHOR: JAWHAR GHOMMAM (e-mail: jawher@squ.edu.om).

This work was supported in part by OmanTel under Grant EG/SQUOT/DVC/CIR/25/207 and in part by Ecole de technologie superieure (ETS).

ABSTRACT Accurate control-oriented composite hydrodynamic parameter knowledge is essential for high-performance control of uncrewed surface vessels, yet conventional identification methods rely on persistent excitation (PE), which is often impractical in real operations. This article proposes an integrated framework combining online parameter estimation with prescribed-time line-of-sight cascade guidance control. The estimation scheme uses dynamic regressor extension and mixing to decouple a 14-parameter composite dynamic model into independent scalar regressions, followed by a prescribed-time least-squares estimator that guarantees practical prescribed-time convergence under bounded disturbances and exact prescribed-time convergence in the disturbance-free case of the estimation errors at a user-defined time. The approach requires only finite excitation from standard maneuvers, eliminating the need for PE. Leveraging these estimates, a prescribed-time cascade guidance controller is developed to achieve precise velocity tracking, with adaptive compensation for unknown disturbances. The framework ensures practical prescribed-time stability of both the composite parameter estimation errors and the tracking errors, independent of initial conditions. Theoretical analysis and experimental results validate the approach, demonstrating accurate composite parameter identification and high-precision tracking under realistic operating conditions.

INDEX TERMS Adaptive control, blackRobotic uncrewed surface vessel (USV), cascade guidance control, dynamic regressor extension and mixing (DREM), parameter estimation, prescribed-time control, prescribed-time line-of-sight (PT-LOS) guidance.

I. INTRODUCTION

Uncrewed surface vessels (USVs) play an increasingly important role in a wide range of marine applications due to their flexibility, low operational cost, and ability to operate in hazardous or inaccessible environments. Their maneuvering capabilities are particularly critical in missions that require precise path-following and rapid response to dynamic conditions. In many practical scenarios, immediate and accurate tracking of a desired path is essential. For instance, in environmental monitoring [34], [43], USVs must follow predefined trajectories to ensure proper spatial data coverage; in search and rescue operations [16], [23], [41], rapid maneuvering is required to reach targets in minimal time; in offshore inspection and surveillance [13], [22], vessels must accurately track pipelines or infrastructure while compensating for disturbances; and in military or security missions [7], real-time trajectory adaptation is crucial for interception and threat avoidance. These applications highlight the necessity for high-performance guidance and control systems capable of ensuring fast, reliable, and precise maneuvering under uncertain and time-varying conditions.

A wide range of approaches have been developed to address parameter estimation problems, including classical techniques, such as linear least squares, maximum likelihood

© 2026 The Authors. This work is licensed under a Creative Commons Attribution 4.0 License. For more information, see https://creativecommons.org/licenses/by/4.0/

estimation, Bayesian regression, and principal component regression [37], [44]. These methods typically require comprehensive statistical information about the process and are, therefore, primarily suited for offline identification. In contrast, adaptive control and system identification frameworks provide various online estimation strategies [2], [8], [36], [38]. However, the applicability of many of these approaches fundamentally relies on the persistent excitation (PE) condition [12], [26], which ensures parameter convergence through asymptotic statistical properties. Achieving high-performance control of USVs, however, critically depends on accurate knowledge of hydrodynamic parameters, which are inherently uncertain and often vary with operating conditions. Traditional identification techniques that rely on PE [1], [5], [35] become difficult to implement in practice, as mission-oriented maneuvers rarely provide sufficiently rich excitation. This limitation significantly restricts the practical applicability of conventional estimation methods in real-world maritime operations.

In light of the restrictive nature of the PE condition, considerable research efforts have been directed toward the development of alternative estimation frameworks capable of ensuring parameter convergence under weaker excitation requirements. Among these, composite learning strategies have emerged as an effective solution [30], [31], [32], combining feedback-based adaptation with prediction-error mechanisms. In such approaches, a virtual system constructed using estimated parameters is employed to generate auxiliary prediction errors, enabling convergence under interval excitation (IE), which imposes significantly milder conditions compared to classical PE. In parallel, concurrent learning techniques offer another promising direction by leveraging recorded data from past system trajectories [21], [33], [46]. By integrating this historical information into the adaptation process, these methods enrich the available excitation, thereby facilitating parameter convergence even when only finite excitation is present during operation. Collectively, these approaches provide practical alternatives to traditional identification schemes, alleviating the dependence on stringent excitation conditions.

A promising alternative for parameter estimation is the dynamic regressor extension and mixing (DREM) framework [4], [17], [28], which decouples estimation dynamics. DREM augments the original regression via filtering or delay operators, reformulating the vector problem into independent scalar regressions. A key advantage is its relaxed excitation requirement: convergence is guaranteed if the determinant of the extended regressor is nonsquare-integrable, removing the need for PE, although this condition is not generally equivalent to PE unless linear time-invariant extensions are used. Subsequent works have shown that even weaker excitation conditions are sufficient, with explicit lower bounds on excitation [11]. Efforts have also focused on accelerating convergence, leading to finite- and predefined-time DREM-based estimators [19], [39]. However, in the presence of bounded disturbances, most existing approaches can only guarantee practical convergence to a residual neighborhood rather than exact convergence to the true parameters.

Although DREM relaxes excitation requirements and enables decoupled estimation, its application to marine systems, particularly USV composite dynamic parameter estimation, remains limited. Existing works mainly address generic systems and ensure only asymptotic convergence, which is inadequate for time-critical marine operations. In practice, the composite dynamic parameters associated with hydrodynamic effects vary significantly due to disturbances, such as waves, currents, and payload changes, complicating identification. Therefore, extending DREM to achieve faster convergence and robustness in such environments remains an important open problem.

Furthermore, the integration of DREM-based estimators into real-time control frameworks for marine applications remains limited. Many existing implementations are validated primarily through theoretical analysis or simulation studies [11], [19], [39], with insufficient emphasis on real-time deployment and computational constraints associated with onboard systems. This gap highlights the need for developing DREM-based identification schemes that are not only robust to marine uncertainties but also suitable for real-time implementation in practical USV platforms.

Overall, existing DREM-based adaptive estimators significantly relax the classical PE requirement by exploiting IE; however, they generally guarantee only asymptotic parameter convergence. Conversely, prescribed-time estimation methods provide convergence within a user-defined time but typically retain PE requirements. The proposed framework combines the advantages of both approaches by integrating DREM with a prescribed-time least-squares (PT-LS) estimator, thereby guaranteeing prescribed-time parameter convergence from a finite interval of excitation. This distinction motivates the proposed methodology and is summarized by the following contributions.

The main contributions of the research can be summarized as follows.

1) A combined estimation framework integrating DREM and a PT-LS estimator is proposed. DREM decouples the 14-parameter USV identification into scalar regressions, while PT-LS ensures practical prescribed-time convergence under bounded disturbances and exact prescribed-time convergence in the disturbance-free case at a user-defined time T from a finite interval of excitation. Unlike the discrete-time fixed-time method in [19], the proposed continuous-time approach guarantees prescribed-time practical convergence of the parameter estimation and tracking errors. Unlike the gradient-based update in [19], PT-LS employs a strong consistency mechanism, ensuring unbiased convergence under bounded disturbances.
2) Unlike the machine learning approach in [10], which relies on offline least-squares support vector machine and particle swarm optimization, the proposed method

operates fully online for real-time parameter adaptation. While [10], [21], [33] requires persistently rich maneuvering data, the present framework only assumes IE. Moreover, it guarantees practical prescribed-time convergence under bounded disturbances, while exact prescribed-time convergence is recovered in the disturbance-free case at a user-defined time T, whereas machine learning methods achieve only asymptotic or data-dependent convergence. This makes it well suited for mission-critical applications requiring reliable estimation within a guaranteed time.

3) Unlike the asymptotic LOS controller in [24], the proposed prescribed-time cascade guidance law ensures practical convergence of the velocity tracking error to a neighborhood of zero at a user-defined time T, independent of initial conditions. It further leverages DREM-PT-LS-based parameter estimates for accurate feedforward compensation and introduces an adaptation law with smooth saturation to ensure robustness while preserving prescribed-time convergence.
4) Beyond the individual use of DREM, prescribed-time estimation, and LOS guidance, the main novelty lies in their unified integration within a continuous-time closed-loop framework for real-time USV applications. In particular, the proposed method combines IE-based DREM identification, a filterless PT-LS estimator with strong consistency correction, and prescribed-time LOS guidance into a single experimentally validated architecture implemented on a real blackBoat USV platform through real-time MAVLink communication and online MATLAB execution.

The rest of this article is organized as follows. Section II presents the modeling of the USV, formulates the problem of identification and control, with some relevant lemmas and definitions useful for the stability analysis. Section III presents the DREM combined with PT-LS estimation algorithm. Section IV outlines the design of the prescribed-time cascaded guidance LOS control algorithm. Section V validates the approach through experimental tests. Finally, Section VI concludes this article.

II. PROBLEM FORMULATION AND PRELIMINARIES

A. DYNAMIC MODEL OF THE USV

Most surface vessel models are formulated based on the three-degree-of-freedom (3-DOF) framework [14]

$$\begin{aligned}\dot{\boldsymbol{\eta}} &= \mathbf{R}(\psi)\boldsymbol{\nu}\\ \mathbf{M}\dot{\boldsymbol{\nu}} &= -\mathbf{C}(\boldsymbol{\nu})\boldsymbol{\nu} - \mathbf{D}(\boldsymbol{\nu})\boldsymbol{\nu} + \boldsymbol{\tau} + \boldsymbol{d}\end{aligned} \tag{1}$$

where $\boldsymbol{\eta} = \left[x, y, \psi\right] \in \mathbb{R}^3$ denotes the Earth-fixed position and heading, where x and y are the inertial-frame coordinates and ψ is the yaw angle. $\boldsymbol{\nu} = \left[u, v, r\right] \in \mathbb{R}^3$ denotes the body-fixed velocity vector, where u, v, and r represent the surge velocity, sway velocity, and yaw rate, respectively. $\boldsymbol{\tau} = [\tau_u,\ 0,\ \tau_r]^\top$ is the control input vector, and $\boldsymbol{d} = [d_u,\ d_v,\ d_r]^\top$ represents bounded external disturbances. The rotation matrix $\mathbf{R}(\psi) = \mathrm{diag}(\boldsymbol{R}_p, 1)$ and the inertia matrix are given by

$$\mathbf{R}_p(\psi) = \begin{bmatrix}\cos\psi & -\sin\psi\\ \sin\psi & \cos\psi\end{bmatrix}, \mathbf{M} = \begin{bmatrix}m_{11} & 0 & 0\\ 0 & m_{22} & m_{23}\\ 0 & m_{32} & m_{33}\end{bmatrix}. \tag{2}$$

The inertia matrix inverse can be expressed as

$$\mathbf{M}^{-1} = \begin{bmatrix}m_{11}^* & 0 & 0\\ 0 & m_{22}^* & m_{23}^*\\ 0 & m_{32}^* & m_{33}^*\end{bmatrix} = \begin{bmatrix}\frac{1}{m_{11}} & 0 & 0\\ [1.2ex]0 & \frac{m_{33}}{\Delta_M} & -\frac{m_{23}}{\Delta_M}\\ [1.2ex]0 & -\frac{m_{32}}{\Delta_M} & \frac{m_{22}}{\Delta_M}\end{bmatrix} \tag{3}$$

where

$$\Delta_M = m_{22}m_{33} - m_{23}m_{32}.$$

The Coriolis–centripetal matrix is

$$\mathbf{C}(\boldsymbol{\nu}) = \begin{bmatrix}0 & 0 & -m_{22}v - m_{23}r\\ 0 & 0 & m_{11}u\\ m_{22}v + m_{23}r & -m_{11}u & 0\end{bmatrix} \tag{4}$$

and the hydrodynamic damping matrix is

$$\mathbf{D}(\boldsymbol{\nu}) = \begin{bmatrix}d_{11}(u) & 0 & 0\\ 0 & d_{22}(v,r) & d_{23}(v,r)\\ 0 & d_{32}(v,r) & d_{33}(v,r)\end{bmatrix} \tag{5}$$

with

$$\begin{aligned}d_{11}(u) &= -X_u - X_{|u|u}|u|\\ d_{22}(v,r) &= -Y_v - Y_{|v|v}|v| - Y_{|r|v}|r|\\ d_{23}(v,r) &= -Y_r - Y_{|v|r}|v| - Y_{|r|r}|r|\\ d_{32}(v,r) &= -N_v - N_{|v|v}|v| - N_{|r|v}|r|\\ d_{33}(v,r) &= -N_r - N_{|v|r}|v| - N_{|r|r}|r|.\end{aligned} \tag{6}$$

The parameters X_u, $X_{|u|u}$, Y_v, Y_r, N_v, and N_r represent the linear hydrodynamic damping derivatives associated with surge, sway, and yaw motions, respectively, while $X_{|u|u}$, $Y_{|v|v}$, $Y_{|r|v}$, $Y_{|v|r}$, $Y_{|r|r}$, $N_{|v|v}$, $N_{|r|v}$, $N_{|v|r}$, and $N_{|r|r}$ denote the corresponding nonlinear (quadratic) damping coefficients. These coefficients capture viscous drag effects and fluid-structure interactions, including both self-damping terms and cross-coupled effects between sway velocity and yaw rate. Specifically, the terms involving $|v|$ and $|r|$ account for nonlinear hydrodynamic resistance that becomes significant at higher velocities, while the cross-coupling coefficients describe the interaction between lateral motion and rotational dynamics.

Accordingly, the kinematic and dynamic equations of the USV can be combined into the following state-space representation:

$$\begin{aligned}\dot{x} &= u\cos\psi - v\sin\psi\\ \dot{y} &= u\sin\psi + v\cos\psi\\ \dot{\psi} &= r\\ \dot{\boldsymbol{\nu}} &= \begin{bmatrix} f_u(\boldsymbol{\nu}) + m_{11}^*(\tau_u + d_u)\\ f_v(\boldsymbol{\nu}) + m_{23}^*(\tau_r + d_r) + m_{22}^* d_v\\ f_r(\boldsymbol{\nu}) + m_{33}^*(\tau_r + d_r) + m_{32}^* d_v\end{bmatrix}\end{aligned} \tag{7}$$

where

$$f_u(\boldsymbol{\nu}) = m_{11}^* m_{22} vr + m_{11}^* m_{23} r^2 + m_{11}^* X_u u + m_{11}^* X_{|u|u}|u|u \tag{8}$$

$$\begin{aligned}f_v(\boldsymbol{\nu}) = {} & \left(m_{23}^* m_{11} - m_{23}^* m_{22}\right) uv - \left(m_{23}^* m_{23} + m_{22}^* m_{11}\right) ur\\ & + \left(m_{22}^* Y_v + m_{23}^* N_v\right) v + \left(m_{22}^* Y_r + m_{23}^* N_r\right) r\\ & + \left(m_{22}^* Y_{|v|v} + m_{23}^* N_{|v|v}\right) |v|v\\ & + \left(m_{22}^* Y_{|r|v} + m_{23}^* N_{|r|v}\right) |r|v\\ & + \left(m_{22}^* Y_{|v|r} + m_{23}^* N_{|v|r}\right) |v|r\\ & + \left(m_{22}^* Y_{|r|r} + m_{23}^* N_{|r|r}\right) |r|r\end{aligned} \tag{9}$$

and

$$\begin{aligned}f_r(\boldsymbol{\nu}) = {} & \left(m_{33}^* m_{11} - m_{33}^* m_{22}\right) uv - \left(m_{33}^* m_{23} + m_{32}^* m_{11}\right) ur\\ & + \left(m_{32}^* Y_v + m_{33}^* N_v\right) v + \left(m_{32}^* Y_r + m_{33}^* N_r\right) r\\ & + \left(m_{32}^* Y_{|v|v} + m_{33}^* N_{|v|v}\right) |v|v\\ & + \left(m_{32}^* Y_{|r|v} + m_{33}^* N_{|r|v}\right) |r|v\\ & + \left(m_{32}^* Y_{|v|r} + m_{33}^* N_{|v|r}\right) |v|r\\ & + \left(m_{32}^* Y_{|r|r} + m_{33}^* N_{|r|r}\right) |r|r.\end{aligned} \tag{10}$$

The nonlinear dynamic model in (7) is widely adopted in the literature for the control of marine vehicles. In this formulation, the position of the vessel, defined at the origin of the body-fixed frame $p := [x\ y]^\top$, is typically selected as the control output. However, as can be observed from the dynamic equations, the system is underactuated due to the absence of a direct control input in the sway direction. Specifically, the sway velocity v cannot be directly influenced by the available control inputs, which are limited to surge force and yaw moment.

B. HAND-POSITION TRANSFORMATION

To facilitate controller design for the underactuated vehicle, define a virtual point located at a distance $\varepsilon > 0$ ahead of the body-fixed origin

$$\bar{\boldsymbol{\eta}}_1 = \begin{bmatrix}\bar{x}\\ \bar{y}\end{bmatrix} = \begin{bmatrix}x + \varepsilon\cos\psi\\ y + \varepsilon\sin\psi\end{bmatrix}. \tag{11}$$

Taking the double differentiation of (11) and using the first three equations of (7) yields

$$\begin{aligned}\ddot{\bar{x}} &= F_x(V) + m_{11}^*\tau_u\cos\psi - \left(m_{23}^* + \varepsilon m_{33}^*\right)\tau_r\sin\psi + d_x\\ \ddot{\bar{y}} &= F_y(V) + m_{11}^*\tau_u\sin\psi + \left(m_{23}^* + \varepsilon m_{33}^*\right)\tau_r\cos\psi + d_y\end{aligned} \tag{12}$$

where $V = [\boldsymbol{\nu}^\top, \psi]^\top$ and

$$\begin{aligned}g_x(V) &= ur\sin\psi + (vr + \varepsilon r^2)\cos\psi\\ g_y(V) &= ur\cos\psi - (vr + \varepsilon r^2)\sin\psi\\ F_x(V) &= f_u(\boldsymbol{\nu})\cos\psi - \left(f_v(\boldsymbol{\nu}) + \varepsilon f_r(\boldsymbol{\nu})\right)\sin\psi - g_x(V)\\ F_y(V) &= f_u(\boldsymbol{\nu})\sin\psi + \left(f_v(\boldsymbol{\nu}) + \varepsilon f_r(\boldsymbol{\nu})\right)\cos\psi + g_y(V)\end{aligned} \tag{13}$$

and the transformed disturbances are

$$\begin{aligned}d_x = {} & m_{11}^* d_u\cos\psi - \left(m_{22}^* + \varepsilon m_{32}^*\right) d_v\sin\psi\\ & - \left(m_{23}^* + \varepsilon m_{33}^*\right) d_r\sin\psi\\ d_y = {} & m_{11}^* d_u\sin\psi + \left(m_{22}^* + \varepsilon m_{32}^*\right) d_v\cos\psi\\ & + \left(m_{23}^* + \varepsilon m_{33}^*\right) d_r\cos\psi.\end{aligned} \tag{14}$$

By defining $\bar{\boldsymbol{\eta}}_2 = \dot{\bar{\boldsymbol{\eta}}}_1$, and $\boldsymbol{\vartheta} = \left[m_{11}^*, m_{23}^* + \varepsilon m_{33}^*\right]^\top$ the transformed system can be compactly written as

$$\begin{aligned}\dot{\bar{\boldsymbol{\eta}}}_1 &= \bar{\boldsymbol{\eta}}_2,\\ \dot{\bar{\boldsymbol{\eta}}}_2 &= \mathbf{J}(\psi)\,\mathrm{diag}(\boldsymbol{\vartheta})\,\bar{\boldsymbol{\tau}} + \mathbf{F}(\chi) + \boldsymbol{d}_\eta\end{aligned} \tag{15}$$

where

$$\mathbf{J}(\psi) = \begin{bmatrix}\cos\psi & -\sin\psi\\ \sin\psi & \cos\psi\end{bmatrix},\quad \boldsymbol{\vartheta} = \begin{bmatrix}\vartheta_1\\ \vartheta_2\end{bmatrix} = \begin{bmatrix}m_{11}^*\\ m_{23}^* + \varepsilon m_{33}^*\end{bmatrix}$$

$$\bar{\boldsymbol{\tau}} = \begin{bmatrix}\tau_u\\ \tau_r\end{bmatrix},\quad \mathbf{F}(\chi) = \begin{bmatrix}F_x(\chi)\\ F_y(\chi)\end{bmatrix},\quad \boldsymbol{d}_\eta = \begin{bmatrix}d_x\\ d_y\end{bmatrix}.$$

Assumption 1: The external disturbance $\boldsymbol{d}_\eta$ is bounded. There exists an unknown bound $\chi > 0$, such that $\|\boldsymbol{d}_\eta\| \le \chi$.

Assumption 2: The inertial matrix $\boldsymbol{M}$ is known, the damping and Coriolis matrices $\boldsymbol{D}(\boldsymbol{\nu})$ and $\boldsymbol{C}(\boldsymbol{\nu})$ are unknown.

Remark 1: Assumption 1 ensures that the effect of environmental disturbances and unmodeled dynamics remains bounded, which is required to establish robustness and practical prescribed-time convergence of the proposed estimator and controller. Assumption 2 reflects the practical situation where the inertial parameters of the USV are known from physical measurements, while the hydrodynamic damping and Coriolis terms remain uncertain and are, therefore, estimated online using the proposed DREM-PT-LS framework.

C. PROBLEM FORMULATION

Accurate knowledge of marine vehicle dynamics is essential for high-performance control. While physical parameters can be measured, hydrodynamic coefficients, especially damping and cross-coupling terms are difficult to obtain due to complex fluid–structure interactions. Traditional methods,

such as towing tank tests and computational fluid dynamics, are costly and impractical for small-scale USVs. This work develops an online framework to estimate a composite regression parameter vector $\boldsymbol{\Theta} \in \mathbb{R}^p$, whose entries comprise both known inertial combinations and unknown hydrodynamic combinations arising from the control-oriented regression reformulation directly from input–output data during normal operation. The considered parameter vector does not necessarily correspond to the original physical hydrodynamic coefficients, but rather to composite quantities arising from the regression reformulation used for control-oriented identification. The system is expressed in a linearly parameterized form $\mathbf{Y}(t) = \boldsymbol{\Phi}^\top(t)\boldsymbol{\Theta} + \mathbf{d}(t)$, where $\mathbf{Y}(t) \in \mathbb{R}^2$ is measurable, $\boldsymbol{\Phi}(t) \in \mathbb{R}^{2\times p}$ is known, and $\mathbf{d}(t)$ is bounded. The objective is to design an estimator $\hat{\boldsymbol{\Theta}}(t)$ such that the error $\tilde{\boldsymbol{\Theta}}(t) = \hat{\boldsymbol{\Theta}}(t) - \boldsymbol{\Theta}$ remains bounded and achieves prescribed-time convergence in the disturbance-free case, while ensuring practical prescribed-time convergence to a small neighborhood of zero in the presence of bounded disturbances and under suitable excitation conditions. The estimated composite dynamic parameters are then used for adaptive control to enhance tracking performance and robustness against uncertainties and disturbances.

D. PRELIMINARIES

Definition 1 (see [27]): A continuous function $\beta : [0, c) \times [0, T) \to [0, \infty)$ is said to belong to class $\mathcal{KL}^e_T$ if, for each fixed s, the mapping $\beta(r, s)$ belongs to class $\mathcal{K}_\infty$ with respect to r and, for each fixed r, the mapping $\beta(r, s)$ is decreasing with respect to s and satisfies $\beta(r, s) \to 0$ as $s \to T$.

Definition 2 (see [45]): Consider the nonlinear system

$$\dot{\boldsymbol{x}}(t) = \boldsymbol{f}(t, x(t)), \quad t \geq 0, \quad \boldsymbol{x}(0) = \boldsymbol{x}_0, \ x \in \mathbb{R}^k \tag{16}$$

where $\boldsymbol{x}(t; x_0)$ denotes the system state and $\boldsymbol{f} : \mathbb{R}^k \to \mathbb{R}^k$ is a continuous function satisfying $f(t, 0) = 0$. The system is said to achieve practical prescribed-time stability (PPTS) if, for any initial condition $\boldsymbol{x}_0 \in \mathbb{R}^k$, there exist a prescribed-time $T_p > 0$ and a constant $\delta > 0$ such that

$$\|\boldsymbol{x}(t; x_0)\| \leq \delta \quad \forall t \geq T_p \tag{17}$$

where δ is a user-defined bound determined by design requirements.

Definition 3 (see [18]): Let $T > 0$, $t_0 \geq 0$, and $m > 0$. A time-varying function $\mu : [t_0, t_0 + T) \to \mathbb{R}_{>0}$ is called a prescribed-time scaling function if it is defined as

$$\mu(t) = \begin{cases} \left(\frac{T}{t_0+T-t}\right)^m, & t \in \mathcal{T}_p \triangleq [t_0, t_0 + T) \\ [1ex]1, & t \geq t_0 + T \end{cases} \tag{18}$$

$$\dot{\mu}(t) = \begin{cases} \frac{m}{T}\,\mu^{1+\frac{1}{m}}(t), & t \in \mathcal{T}_p \triangleq [t_0, t_0 + T) \\ [2ex]0, & t \geq t_0 + T \end{cases} \tag{19}$$

and satisfies the following properties:

1) $\mu(t) > 0$ for all $t \in [t_0, t_0 + T)$;
2) $\mu(t)$ is continuous and strictly increasing on $[t_0, t_0 + T)$; and
3) $\mu(t) \to +\infty$ as $t \to t_0 + T^-$.

This function is used to introduce a time-varying gain that enforces prescribed-time convergence at the predefined time $t_0 + T$.

Lemma 1 (see [47]): If there exists a Lyapunov function $V(t)$ for the system (16) along with positive constants q and δ_0 such that

$$\dot{V}(t) \leq -q\mu(t)V(t) + \delta_0. \tag{20}$$

Then, system (16) is said to satisfy the PPTS.

The following lemma presents a generalized result on prescribed-time stability for cascaded systems. Its proof is provided in the Appendix.

Lemma 2: Consider the following cascade nonlinear system:

$$\dot{\boldsymbol{x}} = \boldsymbol{f}(t, x, \mu(t)) + \boldsymbol{g}(t, x, \mu(t), \xi_e(t)) \tag{21}$$

where $\boldsymbol{x} \in \mathbb{R}^n$, $\boldsymbol{\xi}_e \in \mathbb{R}^n$, and $\mu(t)$ is as given in Definition 3.

The solution $\boldsymbol{x}(t)$ converges to a neighborhood of zero at the prescribed-time $t_0 + T$ (i.e., the system is practical prescribed-time stable with respect to $\boldsymbol{\xi}_e$) if there exist constants $c_1 > 2$, $c_2 > 0$, and a $\mathcal{K}_\infty$ function $\sigma_r(\cdot)$ such that the following assumptions hold.

A) There exists a Lyapunov function $V(\mu(t), \boldsymbol{x})$ satisfying

$$\underline{\alpha}(\mu)\|\boldsymbol{x}\|^2 \leq V(\mu, \boldsymbol{x}) \leq \bar{\alpha}(\mu)\|\boldsymbol{x}\|^2$$
$$\left\| \frac{\partial V}{\partial \boldsymbol{x}} \right\| \leq \mu^{\frac{m+1}{m}} \|\boldsymbol{x}\| \tag{22}$$

and along the f-dynamics

$$\frac{\partial V}{\partial \mu}\dot{\mu} + \frac{\partial V}{\partial x}\boldsymbol{f}(t, \boldsymbol{x}, \mu(t)) \leq -c_1\mu^{\frac{1}{m}}V(\mu(t), \boldsymbol{x}) \tag{23}$$

where $\underline{\alpha}, \bar{\alpha} \in \mathcal{K}_\infty$.

B) The interconnection term $\boldsymbol{g}(t, \boldsymbol{x}, \mu(t), \boldsymbol{\xi}_e(t))$ satisfies

$$\|\boldsymbol{g}(t, \boldsymbol{x}, \mu(t), \boldsymbol{\xi}_e(t))\| \leq c_2\|\boldsymbol{\xi}_e\|. \tag{24}$$

C) The signal $\boldsymbol{\xi}_e$ is practical prescribed-time stable, i.e., for any given $\delta > 0$, there exists a class $\mathcal{KL}^e_T$ function β_ξ such that:

$$\|\boldsymbol{\xi}_e(t)\| \leq \beta_\xi(\|\boldsymbol{\xi}_e(t_0)\|, t - t_0) + \delta \quad \forall t \in \mathcal{T}_p \tag{25}$$

and $\lim_{t\to t_0+T} \|\boldsymbol{\xi}_e(t)\| \leq \delta$.

D) The interconnection gains satisfy the following scaling condition: there exists a $\mathcal{K}_\infty$ function $\sigma_s(\mu)$ such that:

$$\frac{d\sigma_s(\mu)}{d\mu} \leq \frac{1}{2m}\mu^{-1-\frac{1}{m}}\sigma_s(\mu)\bar{\alpha}_s(\mu) \tag{26}$$

where $\bar{\alpha}_s(\mu)$ is the prescribed-time convergent gain for the x-dynamics, and

$$\sigma_s(\mu)c_2^2 = \mathcal{S}[\exp(c_1)\bar{\alpha}_s(\mu)] \tag{27}$$

meaning $\sup_{\mu\in\mathbb{R}_p} \dfrac{\sigma_s(\mu)c_2^2}{\exp(c_1)\bar{\alpha}_s(\mu)} < \infty$, where $\mathbb{R}_p \triangleq [1, \infty)$.

Then, for any initial condition $\boldsymbol{x}(t_0)$ and $\boldsymbol{\xi}_e(t_0)$, and for any given $\varepsilon > 0$, there exist functions $\beta_x \in \mathcal{KL}_T^e$, a finite constant $\epsilon > 0$, and a sufficiently small $\delta > 0$ such that

$$\|\boldsymbol{x}(t)\| \leq \beta_x(\|\boldsymbol{x}(t_0)\|, t - t_0) + \epsilon\delta + \varepsilon \quad \forall t \in \mathcal{T}_p \tag{28}$$

and moreover, $\lim_{t\to t_0+T} \|\boldsymbol{x}(t)\| \leq \epsilon\delta + \varepsilon$, i.e., $x(t)$ converges to a neighborhood of zero whose size can be made arbitrarily small by choosing δ sufficiently small.

Lemma 3 (see [25]): For any $w > 0$ and $x \in \mathbb{R}$, the inequality $0 \leq |\boldsymbol{x}| - \boldsymbol{x}\tanh(\frac{\boldsymbol{x}}{w}) \leq 0.2785\, w$ holds.

Lemma 4 (see[9]): For any vector $\boldsymbol{x} \in \mathbb{R}^n$, there exists a positive scalar $\hbar$ such that $0 \leq \|\boldsymbol{x}\| - \frac{\boldsymbol{x}^\top x}{\sqrt{\boldsymbol{x}^\top \boldsymbol{x} + \hbar^2}} \leq \hbar$.

III. COMPOSITE PARAMETER ESTIMATION BASED ON IMPROVED DREM METHOD

In this section, the objective is to estimate the unknown composite dynamic parameters associated with the hydrodynamic behavior of the USV. To this end, it is necessary to reformulate the system dynamics in (14) into a regression model suitable for parameter estimation. It should be noted that the resulting parameter vector consists of composite quantities obtained from the regression reformulation, rather than the original physical hydrodynamic coefficients themselves. Since the model involves derivatives that are not directly measurable, a linear filtering technique is used. Specifically, consider the first-order stable filter defined by the operator $\frac{\alpha}{s+\alpha}, \quad \alpha > 0$, where $\frac{1}{\alpha}$ represents the filter time constant. Using the identity $\alpha(\boldsymbol{x} - \frac{\alpha}{s+\alpha}\{\boldsymbol{x}\}) = \frac{\alpha}{s+\alpha}\{\dot{\boldsymbol{x}}\}$, the derivative terms can be expressed in terms of measurable signals. Based on this filtering approach, the dynamics in the second equation of (15) can be rearranged into a regression form as follows:

$$\mathbf{Y}(t) = \boldsymbol{\Phi}^\top(t)\boldsymbol{\Theta} + \mathbf{d}(t) \tag{29}$$

where the filtered output vector $\mathbf{Y}(t) \in \mathbb{R}^2$ is defined as

$$\mathbf{Y}(t) = \begin{bmatrix} y_1(t) \\ y_2(t) \end{bmatrix} = \alpha\left(\bar{\boldsymbol{\eta}}_2(t) - \frac{\alpha}{s+\alpha}\{\bar{\boldsymbol{\eta}}_2(t)\}\right). \tag{30}$$

The regressor matrix $\boldsymbol{\Phi}(t) \in \mathbb{R}^{2\times 14}$ is given by $\boldsymbol{\Phi}(t) = \frac{\alpha}{s+\alpha}\{\mathbf{J}(\psi(t))\,\boldsymbol{\Xi}(t)\}$, and the disturbance vector $\boldsymbol{d}(t) = \begin{bmatrix} d_1(t) \\ d_2(t) \end{bmatrix} = \frac{a}{s+a}\{\mathbf{d}_0(t)\}$ where $\boldsymbol{\Xi}(t) = \begin{bmatrix} \phi_1(\boldsymbol{v}(t)) & \mathbf{0}_{1\times 9} \\ \mathbf{0}_{1\times 5} & \phi_2(\boldsymbol{v}(t)) \end{bmatrix}$ and where $\mathbf{d}_0(t)$ includes external disturbances and unmodeled dynamics, given as follows:

$$\mathbf{d}_0(t) = \mathbf{J}(\psi)\begin{bmatrix} u(t)r(t) \\ v(t)r(t) + \varepsilon r^2(t) \end{bmatrix} + \begin{bmatrix} d_x \\ d_y \end{bmatrix}.$$

The basis vectors $\phi_1(.)$ and $\phi_2(.)$ are defined as $\phi_1(\boldsymbol{v}) = \begin{bmatrix} \tau_u & vr & r^2 & u & |u|u \end{bmatrix}$ and $\phi_2(\boldsymbol{v}) = [\tau_r\; uv\; -ur\; v\; r\; |v|v\; |r|v\; |v|r\; |r|r]$, respectively. The unknown parameter vector $\boldsymbol{\Theta} \in \mathbb{R}^{14}$ is defined as

$$\boldsymbol{\Theta} = \begin{bmatrix} m_{11}^* \\ m_{11}^* m_{22} \\ m_{11}^* m_{23} \\ m_{11}^* X_u \\ m_{11}^* X_{|u|u} \\ m_{23}^* + \varepsilon m_{33}^* \\ m_{23}^* m_{11} - m_{23}^* m_{22} + \varepsilon\left(m_{33}^* m_{11} - m_{33}^* m_{22}\right) \\ m_{23}^* m_{23} + m_{22}^* m_{11} + \varepsilon\left(m_{33}^* m_{23} + m_{32}^* m_{11}\right) \\ m_{22}^* Y_v + m_{23}^* N_v + \varepsilon\left(m_{32}^* Y_v + m_{33}^* N_v\right) \\ m_{22}^* Y_r + m_{23}^* N_r + \varepsilon\left(m_{32}^* Y_r + m_{33}^* N_r\right) \\ m_{22}^* Y_{|v|v} + m_{23}^* N_{|v|v} + \varepsilon\left(m_{32}^* Y_{|v|v} + m_{33}^* N_{|v|v}\right) \\ m_{22}^* Y_{|r|v} + m_{23}^* N_{|r|v} + \varepsilon\left(m_{32}^* Y_{|r|v} + m_{33}^* N_{|r|v}\right) \\ m_{22}^* Y_{|v|r} + m_{23}^* N_{|v|r} + \varepsilon\left(m_{32}^* Y_{|v|r} + m_{33}^* N_{|v|r}\right) \\ m_{22}^* Y_{|r|r} + m_{23}^* N_{|r|r} + \varepsilon\left(m_{32}^* Y_{|r|r} + m_{33}^* N_{|r|r}\right) \end{bmatrix}$$

where $\boldsymbol{\Theta} = [\theta_1, \ldots, \theta_{14}]^\top \in \mathbb{R}^{14}$. Equation (29) clearly transforms the parameter estimation problem into a normalized regression form to which the DREM method [3] can be applied.

Remark 2: Although Assumption 2 states that the inertia matrix $\mathbf{M}$ is known, the composite regression vector $\boldsymbol{\Theta}$ retains several coefficients formed exclusively from the entries of $\mathbf{M}$. These coefficients are therefore known constants rather than unknown physical parameters. They are kept in the implemented 14-dimensional regression to preserve the estimator structure used in the numerical and experimental validation. Hence, the adopted parameterization is redundant but algebraically valid. A minimal parameterization could be obtained by moving all known inertial combinations to the known part of the regression and estimating only the hydrodynamic coefficients.

Remark 3: Note that the filtered regression model (29) provides only two output equations, leaving the composite dynamic parameters severely coupled and underdetermined. Traditional least-squares methods would struggle with such coupling, as the convergence of each parameter estimate depends on the behavior of all others, leading to slow and potentially oscillatory convergence. Moreover, the presence of the disturbance term $\mathbf{d}(t)$, which accounts for external forces, such as waves, wind, and unmodeled hydrodynamics, further complicates the estimation task by introducing unknown inputs that can bias the composite parameter estimates if not properly handled.

A. GENERAL DREM METHOD

The DREM method presented in [6] and [29] addresses the challenge of parameter coupling through a two-step procedure that transforms the coupled multiparameter estimation problem into a set of independent scalar estimation problems. The first step, known as regressor extension, artificially increases the number of available equations by

applying a linear bounded-input bounded-output stable operator $\mathcal{H}_j(s) = \frac{\beta_j}{s+\alpha_j}, \beta_j > 0, \alpha_j > 0, \forall j \in \{1, \ldots, q\}$ (seven distinct filters are employed to generate a total of 14 scalar regression equations associated with the composite parameter vector) to (29), yielding the filtered regression $\mathbf{Y}_f^{(j)}(t) = [\mathbf{\Phi}_f^{(j)}(t)]^\top \mathbf{\Theta} + \mathbf{d}_f^{(j)}(t)$, where the filtered output is defined as $\mathbf{Y}_f^{(j)}(t) = \mathcal{H}_j(s)\mathbf{Y}(t) \in \mathbb{R}^2$, the filtered regressor is $\mathbf{\Phi}_f^{(j)}(t) = \mathcal{H}_j(s)\mathbf{\Phi}(t) \in \mathbb{R}^{2\times 14}$, and $\mathbf{d}_f^{(j)}(t) = \mathcal{H}_j(s)\mathbf{d}(t) \in \mathbb{R}^2$.

To construct the extended regression system, seven distinct filters are applied to the original two-dimensional regression model. Since each filtered regression generates two scalar equations, the resulting extended regression contains a total of $2 \times 7 = 14$ scalar equations. Accordingly, the extended system is obtained by stacking the seven filtered output vectors together with the corresponding seven filtered regressor matrices as follows:

$$\mathcal{Y}(t) = \left[\mathbf{Y}_f^{(i)}(t)\right]_{i=1}^{q} \quad \mathcal{F}(t) = \left[\left[\mathbf{\Phi}_f^{(i)}(t)\right]^\top\right]_{i=1}^{q} \tag{31}$$

$$\mathcal{D}(t) = \left[\mathbf{d}_f^{(i)}(t)\right]_{i=1}^{q} \tag{32}$$

where $\mathcal{Y}(t), \mathcal{D}(t) \in \mathbb{R}^{14}$. The extended regression system is then compactly written as

$$\mathcal{Y}(t) = \mathcal{F}(t)\mathbf{\Theta} + \mathcal{D}(t) \tag{33}$$

which transforms the original underdetermined two-output system into a square $2q$-output system, providing exactly as many equations as unknown parameters. The square regressor matrix $\mathcal{F}(t) \in \mathbb{R}^{14\times 14}$ is now amenable to decoupling via the mixing matrix and this makes the second step of the procedure. Premultiplying (33) by the adjugate matrix $\text{adj}(\mathcal{F}(t)) = \det(\mathcal{F})\mathcal{F}^{-1}$, results in

$$\begin{aligned}\mathcal{Y}_{\text{mix}}(t) &= \underbrace{\text{adj}(\mathcal{F}(t))\mathcal{F}(t)}_{\mathbf{\Delta}_{\text{mix}}}\mathbf{\Theta} + \underbrace{\text{adj}(\mathcal{F}(t))\boldsymbol{D}(t)}_{\upsilon_{\text{mix}}} \\ &= \mathbf{\Delta}_{\text{mix}}(t)\mathbf{\Theta} + \upsilon_{\text{mix}}(t)\end{aligned} \tag{34}$$

where $\mathbf{\Delta}_{\text{mix}}(t) \in \mathbb{R}^{2q\times 2q}$ is a diagonal mixing matrix such that $\mathbf{\Delta}_{\text{mix}} = \text{diag}(\lambda_1(t), \ldots, \lambda_{2q}(t))$, where the scalars $\lambda_j(t)$, $j \in \{1, \ldots, 2q\}$ are the diagonal entries of this transformed regressor matrix. By applying the pure least-squares method to each scalar component i of (34), the estimation according to the gradient descent algorithm is obtained as follows:

$$\dot{\hat{\theta}}_i(t) = \gamma_i\lambda_i(t)\left(Y_{\text{mix},i}(t) - \lambda_i(t)\hat{\theta}_i(t)\right) \tag{35}$$

in which $\gamma_i > 0$ is the adaptive gain.

Lemma 5 (see [40]): Consider the linear regression with disturbance (33), after applying the decent gradient algorithm (35). Under the assumption that $\upsilon_{\text{mix},i}$ is bounded and the regressor satisfies the excitation condition $\int_{t_0}^{\infty}\lambda_i(s)ds = \infty$. Then, the estimation error $e_i(t) = \theta_i - \hat{\theta}_i(t)$ satisfies

$$|e_i(t)| \le e^{-\gamma_i\int_{t_0}^{t}\lambda_i^2(\tau)d\tau}|e_i(t_0)| + \sqrt{\frac{\gamma_i}{2}}\sqrt{\int_{t_0}^{t}\upsilon_{\text{mix},i}^2(s)\,ds}.$$

Furthermore if $\|\upsilon_{\text{mix},i}\|_\infty \le \bar{\upsilon}_i$, then the estimation error converges to a residual set: $\limsup_{t\to\infty}|e_i(t)| \le \sqrt{\frac{\gamma_i}{2}}\bar{\upsilon}_i\sqrt{T}$ for any finite T, and the system is input-to-state stable (ISS) with respect to the disturbance.

Remark 4: In marine applications, after excitation maneuvers (e.g., turns or accelerations), control inputs typically return to trim conditions, where motion is dominated by hydrodynamic drag. For small velocities during cruising or station-keeping, drag is approximately linear, leading to exponential decay of surge, sway, and yaw velocities. Consequently, the regressor $\lambda_i(t)$ in (35), formed from velocity terms associated with the composite dynamic parameterization, also decays exponentially, making $\int_{t_0}^{\infty}\lambda_i^2(t)\,dt < \infty$. This violates the convergence condition of the gradient estimator, preventing convergence of the composite parameter estimates to their true values and rendering the classical gradient approach unsuitable for USV identification.

From the discussion above, in order to overcome this limitation, an improved least-squares estimator is to be designed, which will only require that the regressor satisfies the finite-time excitation condition $\int_{t_0}^{t^*}\lambda_i^2(t)\,dt \ge \epsilon_i > 0$ over an initial interval $[t_0, t^*]$, regardless of whether $\lambda_i(t)$ subsequently decays to zero.

B. PARAMETER ESTIMATION BASED ON PT-LS

An important contribution of this work is the realization of the identification of the composite hydrodynamic parameters in prescribed time, meaning that the estimates achieve exact prescribed-time convergence in the disturbance-free case and practical prescribed-time convergence under bounded disturbances at a user-specified time T, independent of initial conditions and without requiring PE. This is achieved through the combination of DREM to decouple the 14 composite parameters into independent scalar regressions, followed by the application of PT-LS estimator that employs a blow-up function $\mu(t) = (T/(t_0 + T - t))^m$ to enforce prescribed-time convergence of the estimation error dynamics. Unlike conventional approaches that rely on asymptotic convergence or PE [3], [6], [17], this framework guarantees prescribed-time practical identification using only an initial excitation interval, making it particularly well suited for USV applications where excitation is naturally limited.

Inspired by the prescribed-time filterless least square control method in [20], a novel estimator for $\hat{\theta}_i(t)$ is proposed as follows:

$$\hat{\theta}_i(t) = \alpha_i(t) + \gamma_i(t)\int_{t_0}^{t}\frac{\mu^2(s)\lambda_i(s)Y_{\text{mix},i}(s)}{1+\mu^2(s)\lambda_i^2(s)}\,ds \tag{36}$$

where $\mu(t)$ is the blow-up function, $\gamma_i(t)$ is a time-varying gain, and $\alpha_i(t)$ is an auxiliary variable. The adaptation gain dynamics are designed as

$$\dot{\gamma}_i(t) = -\gamma_i^2(t)\frac{\mu^2(t)\lambda_i^2(t)}{1+\mu(t)^2\lambda_i^2}, \quad \gamma_i(t_0) > 0. \tag{37}$$

The auxiliary variable $\alpha_i(t)$ is designed to eliminate the need for filtering the regressor derivatives. Its dynamics are

$$\begin{aligned}\dot{\alpha}_i(t) = &-\gamma_i(t)\frac{\mu^2(t)\lambda_i^2(t)}{1+\mu^2(t)\lambda_i^2(t)}\alpha_i(t)\\ &-\frac{2m}{T}\frac{\mu^{1+\frac{1}{m}}(t)\gamma_i(t)}{1+\mu^2(t)\lambda_i^2(t)}\int_{t_0}^{t}\lambda_i(s)Y_{\mathrm{mix},i}(s)\,ds\\ &+c_0\mu(t)\gamma_i(t)\left(S_i^*-\Phi_i^*\hat{\theta}_i(t)\right)\end{aligned} \tag{38}$$

where

$$S_i^* = \int_{t_0}^{t^*}\frac{\lambda_i(s)}{1+\mu^2(s)\lambda_i^2(s)}Y_{\mathrm{mix},i}(s)\,ds \tag{39}$$

and

$$\Phi_i^* = \int_{t_0}^{t^*}\frac{\lambda_i^2(s)}{1+\mu^2(s)\lambda_i^2(s)}\,ds \tag{40}$$

where $t^* \in (t_0, t_0+T)$ denotes the first instant at which the normalized IE condition is satisfied, i.e., $t^* = \inf\{t \in (t_0, t_0+T) : \int_{t_0}^{t}\frac{\lambda_i^2(s)}{1+\mu^2(s)\lambda_i^2(s)}\,ds \geq \epsilon_i\}$, with $\epsilon_i > 0$.

Remark 5: The key difference in [20] is that the original filterless LS estimator uses a matrix gain $\Gamma(t)$ to handle the coupled parameters, whereas the proposed estimator exploits DREM decoupling to replace it with scalar gains $\gamma_i(t)$ for each independent channel. This simplification reduces computational complexity and simplifies implementation while preserving all theoretical guarantees prescribed-time convergence, strong consistency, and robustness to disturbances.

Lemma 6: Consider the scalar regression after DREM decoupling: $Y_{\mathrm{mix},i}(t)=\lambda_i(t)\Theta_i+\upsilon_{\mathrm{mix},i}(t)$, $i=1,\ldots,2q$ where $\lambda_i(t)$ is a known bounded regressor and $\upsilon_{\mathrm{mix},i}(t)$ is a bounded disturbance. Suppose the IE condition holds: $\Phi_i^*(t) \geq \epsilon_i > 0$ for some $t^* < t_0+T$. Then, the prescribed-time filterless least-squares estimator is practically prescribed-time convergent.

Proof: Consider the scalar DREM regression

$$Y_{\mathrm{mix},i}(t) = \lambda_i(t)\theta_i + \upsilon_{\mathrm{mix},i}(t) \tag{41}$$

where θ_i is an unknown constant and $\upsilon_{\mathrm{mix},i}(t)$ is bounded.

Define the normalized quantities

$$\beta_i(t) = \frac{\lambda_i(t)}{1+\mu^2(t)\lambda_i^2(t)}, \qquad a_i(t) = \frac{\lambda_i^2(t)}{1+\mu^2(t)\lambda_i^2(t)}. \tag{42}$$

Using (36)–(38), the estimator dynamics become

$$\dot{\hat{\theta}}_i = -\gamma_i\mu^2 a_i\hat{\theta}_i + c_0\mu\gamma_i\left(S_i^*-\Phi_i^*\hat{\theta}_i\right)+\gamma_i\mu^2\beta_i Y_{\mathrm{mix},i}. \tag{43}$$

Substituting (41) into (39) and given that $\tilde{\theta}_i = \hat{\theta}_i - \theta_i$ gives

$$S_i^* - \Phi_i^*\hat{\theta}_i = -\Phi_i^*\tilde{\theta}_i + d_i^* \tag{44}$$

where

$$d_i^* = \int_{t_0}^{t^*}\beta_i(s)\upsilon_{\mathrm{mix},i}(s)\,ds. \tag{45}$$

Using (41) and (44), the estimation error dynamics become

$$\dot{\tilde{\theta}}_i = -\gamma_i\mu^2 a_i\tilde{\theta}_i - c_0\mu\gamma_i\Phi_i^*\tilde{\theta}_i + c_0\mu\gamma_i d_i^* + \gamma_i\mu^2\beta_i\upsilon_{\mathrm{mix},i}. \tag{46}$$

Consider the Lyapunov function

$$V_i = \frac{1}{2}\gamma_i^{-1}\tilde{\theta}_i^2. \tag{47}$$

From (37), we have $\dot{\gamma}_i^{-1} = \mu^2 a_i$. Differentiating (47) and using (46) yields

$$\begin{aligned}\dot{V}_i = &-\frac{1}{2}\mu^2 a_i\tilde{\theta}_i^2 - c_0\mu\Phi_i^*\tilde{\theta}_i^2\\ &+c_0\mu d_i^*\tilde{\theta}_i + \mu^2\beta_i\tilde{\theta}_i\upsilon_{\mathrm{mix},i}.\end{aligned} \tag{48}$$

Applying Young's inequality gives

$$c_0\mu d_i^*\tilde{\theta}_i \leq \frac{c_0\mu\Phi_i^*}{2}\tilde{\theta}_i^2 + \frac{c_0\mu}{2\Phi_i^*}(d_i^*)^2 \tag{49}$$

$$\mu^2\beta_i\tilde{\theta}_i\upsilon_{\mathrm{mix},i} \leq \frac{1}{2}\mu^2 a_i\tilde{\theta}_i^2 + \frac{1}{2}\frac{\mu^4\beta_i^2}{a_i}\upsilon_{\mathrm{mix},i}^2. \tag{50}$$

Since $\frac{\mu^4\beta_i^2}{a_i} = \frac{\mu^4}{1+\mu^2\lambda_i^2}$, and assuming $|\lambda_i(t)| \geq \frac{c_\lambda}{\mu(t)}$, one obtains $\frac{\mu^4\beta_i^2}{a_i} \leq \frac{1}{c_\lambda^2}$. Therefore

$$\dot{V}_i \leq -\frac{c_0}{2}\mu\Phi_i^*\tilde{\theta}_i^2 + \frac{c_0\mu}{2\Phi_i^*}(d_i^*)^2 + \frac{1}{2c_\lambda^2}\upsilon_{\mathrm{mix},i}^2. \tag{51}$$

Under the IE condition $\Phi_i^* \geq \epsilon_i > 0$ and using $\tilde{\theta}_i^2 = 2\gamma_i V_i$, it follows that

$$\dot{V}_i \leq -c_0\mu\epsilon_i\gamma_i V_i + \frac{c_0\mu}{2\epsilon_i}(d_i^*)^2 + \frac{1}{2c_\lambda^2}\upsilon_{\mathrm{mix},i}^2. \tag{52}$$

Note here the term $\frac{c_0\mu(t)}{2\epsilon_i}(d_i^*)^2$ is associated with the finite stored disturbance over the excitation interval $[t_0, t^*]$. In practice, due to the normalization introduced in the estimator and the finite integration horizon, d_i^* can be made sufficiently small such that the stabilizing term proportional to $-\mu(t)V_i$ dominates the residual perturbation. Consequently, the estimation error converges to an arbitrarily small neighborhood of the origin in prescribed time. Hence, the estimator guarantees PPTS. Moreover, if $d_i^* = 0$, $\upsilon_{\mathrm{mix},i}(t) = 0$, then $\dot{V}_i \leq -c_0\mu\epsilon_i\gamma_i V_i$, which implies $\lim_{t\to t_0+T}\tilde{\theta}_i(t) = 0$.

Remark 6: The mixed disturbance term $\upsilon_{\mathrm{mix},i}(t)$ can be eliminated after a finite time by incorporating a predefined-time disturbance observer similar to [42]. In this case, the disturbance estimation error vanishes for $t \geq T_c$, yielding $\upsilon_{\mathrm{mix},i}(t) = 0$. Consequently, the estimator error dynamics become disturbance-free after T_c, allowing exact prescribed-time convergence beyond the observer convergence time.

Remark 7: Through the DREM method and the prescribed-time filterless least-squares updating law, it becomes possible to estimate the 14 composite hydrodynamic dynamic parameters of the USV using only conventional maneuvers under a limited IE condition. This breakthrough relies solely on information from the filtered regression model

(29), constructed from standard onboard sensor measurements. The framework guarantees exact prescribed-time convergence in the disturbance-free case and practical prescribed-time convergence under bounded disturbances at a user-specified time T, requiring only that the regressor satisfy $\int_{t_0}^{t} \frac{\lambda_i^2(s)}{1+\mu^2(s)\lambda_i^2(s)}\, ds \geq \epsilon_i > 0$ over a finite initial window $[t_0, t^*]$, a condition easily met by brief, conventional maneuvers such as turns and accelerations. This significantly relaxes the stringent PE requirements of traditional methods.

Remark 8: Although the PT-LS estimator ensures prescribed-time convergence under suitable excitation and full-rank regression conditions, simultaneous identification of all USV composite hydrodynamic parameters is difficult in practice. This is due to regressor coupling, unequal excitation levels, and strong correlation among some nonlinear basis functions. Therefore, a staged PT-LS strategy is adopted, where a subset of dominant parameters is estimated first while the remaining estimates are temporarily frozen. Once the first subset converges, the estimator is reinitialized to identify the remaining parameters using a cleaner residual model. This improves numerical conditioning and enables practical convergence of the full parameter vector.

C. DISCUSSION ON PARAMETER TUNING AND PRACTICAL IMPLEMENTATION

The design parameters of the proposed DREM–PT-LS estimator should be selected by balancing convergence speed, excitation richness, and numerical robustness. The prescribed time T should be chosen larger than the expected duration required to collect sufficient IE and sufficiently larger than the sampling period in implementation. A very small T may lead to large values of the prescribed-time scaling function and consequently large transient control or adaptation signals. The exponent m controls the growth rate of $\mu(t)$; larger values accelerate convergence near $t_0 + T$ but increase numerical sensitivity, whereas smaller values provide smoother transients. In practice, moderate values of m are preferred.

The initial gains $\gamma_i(t_0)$ should be selected positive and bounded. Larger values generally improve the initial adaptation rate but may amplify noise, while smaller values yield smoother but slower estimation. The gain c_0 determines the strength of the stored-data correction term. Increasing c_0 accelerates convergence after the IE condition is satisfied, but overly large values may introduce oscillations or sensitivity to measurement noise. Therefore, c_0 should be increased gradually until the desired convergence speed is obtained without excessive control activity.

The excitation instant t^* is not chosen arbitrarily, but is determined online as the first time at which the normalized IE condition is satisfied, namely $t^* = \inf\{t \in (t_0, t_0 + T) : \int_{t_0}^{t} \frac{\lambda_i^2(s)}{1+\mu^2(s)\lambda_i^2(s)}\, ds \geq \epsilon_i\}$. Thus, t^* should occur before the prescribed time $t_0 + T$. In implementation, trajectory segments such as turns, accelerations, or lemniscate maneuvers can be used to enrich the regressor and ensure that the above condition is satisfied sufficiently early. If t^* occurs too close to $t_0 + T$, the prescribed time T should be increased or additional excitation maneuvers should be introduced.

Overall, the parameter selection involves a tradeoff between convergence speed, robustness to disturbances, and sensitivity to measurement noise, and should, therefore, be tuned according to the sensing quality and computational limitations of the target USV platform.

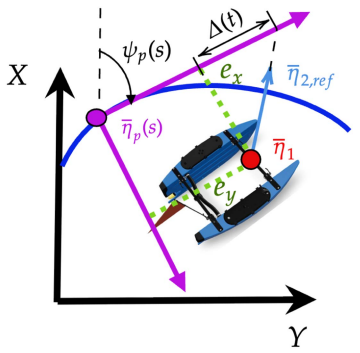

FIGURE 1. Geometry of LOS-based path-following for USVs.

IV. INCORPORATING WITH ADAPTIVE PRESCRIBED-TIME PATH FOLLOWING CONTROLLER

In the following, a prescribed-time line-of-sight (PT-LOS) algorithm is designed in such a way that the PT-LS estimator is seamlessly integrated into the closed-loop guidance and control framework. Specifically, the estimated hydrodynamic parameters obtained from the PT-LS update law are continuously fed back into the PT-LOS controller to compensate for model uncertainties and improve trajectory tracking performance under external disturbances.

A. PT-LOS GUIDANCE CONTROL

In the following, we delve into the path-following maneuver control problem of the USV, leveraging the outcomes of the parameter estimation stage. The path-following architecture is built upon a LOS guidance law [14, Ch. 11], designed to steer the USV toward a desired path as illustrated in Fig. 1. Assuming the path function is a regular path of class $\mathcal{C}^2$, the path-tangential angle $\psi_p(s) \in \mathbb{R}$ is defined such that $\frac{\partial \bar{\boldsymbol{\eta}}_p(s)}{\partial s} = \|\frac{\partial \bar{\boldsymbol{\eta}}_p(s)}{\partial s}\|[\cos(\psi_p(s)), \sin(\psi_p(s))]^\top$. The path following error is defined as

$$\boldsymbol{e} = [e_x, e_y]^\top = \boldsymbol{R}_p(\psi_p(s))^\top(\bar{\boldsymbol{\eta}}_1 - \bar{\boldsymbol{\eta}}_p(s)). \tag{53}$$

The objective of the guidance law is to provide two key outputs: a reference velocity $\bar{\boldsymbol{\eta}}_{2,\mathrm{ref}}$ and an update law for the path parameter $\dot{s}$. To this end, decompose the inertial velocity

as $\bar{\eta}_2 = \bar{\eta}_{2,\text{ref}} + \tilde{\eta}_2$. The closed-loop dynamics of the path-following kinematics can be written as

$$\begin{aligned}\dot{e} &= \dot{R}_p(\psi_p(s))^\top \left(\bar{\eta}_1 - \bar{\eta}_p(s)\right) + R_p(\psi_p(s))^\top \left(\bar{\eta}_2 - \frac{\partial \bar{\eta}_p(s)}{\partial s}\dot{s}\right) \\ &= \dot{\psi}_p(s) S^\top R_p(\psi_p(s))^\top (\bar{\eta}_1 - \bar{\eta}_p(s)) + R_p(\psi_p(s))^\top (\bar{\eta}_{2,\text{ref}} \\ &\quad + \tilde{\eta}_2 - \frac{\partial \bar{\eta}_p(s)}{\partial s}\dot{s}) \end{aligned} \tag{54}$$

where $S \in \mathfrak{so}(2)$ is a skew symmetric matrix.

Different from [14, Ch. 11] and [24], the reference LOS velocity $\bar{\eta}_{2,\text{ref}}$ and the update law for the path parameter are designed to ensure prescribed-time convergence of the path following error. The modified laws are given as follows:

$$\bar{\eta}_{2,\text{ref}} = \frac{U}{\sqrt{\Delta^2(t) + e_y^2}} R_p(\psi_p(s)) \begin{bmatrix} \Delta(t) \\ -e_y \end{bmatrix} - K_p \mu(t) e \tag{55}$$

$$\begin{aligned}\dot{s} &= U \left(\frac{\Delta(t)}{\sqrt{\Delta^2(t) + e_y^2}} + \frac{e_x}{\sqrt{\Delta^2(t) + e_x^2}} \right) \left\| \frac{\partial \bar{\eta}_p(s)}{\partial s} \right\|^{-1} \\ &\quad + K_s \mu(t) e_x \end{aligned} \tag{56}$$

where $\Delta(t) = \Delta_0 \mu^{-1}(t) = \Delta_0 (\frac{t_0 + T - t}{T})^m$ is the time-varying look-ahead distance and Δ_0 is the initial look-ahead distance. K_p and K_s are positive definite diagonal gain matrices.

Substituting the modified guidance law (55) and (56) into the error dynamics (54) yields

$$\dot{e} = \dot{\psi}_p(s) S^T e - U \begin{bmatrix} \frac{e_x}{\sqrt{\Delta^2(t) + e_x^2}} \\ [6pt] \frac{e_y}{\sqrt{\Delta^2(t) + e_y^2}} \end{bmatrix} - K_p \mu(t) e + R_p(s)^T \tilde{\eta}_2. \tag{57}$$

B. PRESCRIBED-TIME DYNAMIC CONTROLLER

The prescribed-time dynamic controller is to design $\bar{\tau}$ to track the reference guidance velocity $\bar{\eta}_{2,\text{ref}}$. To achieve the prescribed-time tracking objective of the velocity guidance vector, we first introduce the following coordinate transformation $z = \mu(t)\tilde{\eta}_2$. This allows to rewrite the tracking error dynamics as

$$\dot{z} = \frac{\dot{\mu}(t)}{\mu(t)} z + \mu(t) \left(\mathbf{B}\bar{\tau} + \mathbf{Y}^* \Theta + d_\eta - \dot{\bar{\eta}}_{\text{ref},2} \right) \tag{58}$$

where $\mathbf{B}(\psi, \vartheta) = \mathbf{J}(\psi)\,\text{diag}(\vartheta)$ and $Y^* \in \mathbb{R}^{2\times 14}$ is a known regressor matrix. The control input $\bar{\tau}$ can be designed as

$$\begin{aligned} \bar{\tau} &= \mathbf{B}^{-1} \left(-\mathbf{Y}^* \hat{\Theta} + \dot{\bar{\eta}}_{\text{ref},2} - \frac{m}{T} \mu^{1/m}(t) \tilde{\eta}_2 + \mathbf{u}_{\text{PT}} \right) \\ \mathbf{u}_{\text{PT}} &= -\frac{z\, \mathbf{u}_T^\top \mathbf{u}_T}{\sqrt{\|z\|^2 \mathbf{u}_T^\top \mathbf{u}_T + \varepsilon \mu(t)^{-2}}} \\ \mathbf{u}_T &= k_T z + \hat{\chi} \tanh\left(\frac{\mu(t) z}{c_0} \right). \end{aligned} \tag{59}$$

The update law for the unknown bound χ is designed as follows:

$$\dot{\hat{\chi}} = \mu(t) z^\top \tanh\left(\frac{\mu(t) z}{c_0} \right) - \mu(t) c_0 \hat{\chi} + \frac{c_0}{\mu(t)} \hat{\chi} \tag{60}$$

where k_T is a positive control gain, $c_0 = \frac{\bar{c}_0}{\mu(t)}$ is a time varying gain with $\bar{c}_0 > 0$. The main result for the prescribed-time guidance control is presented in the following theorem.

Theorem 1: Consider the transformed USV model (15), under assumptions 1 and 2, the LOS-guidance laws (55) and (56), the control input (59) and the update law (60). The closed-loop signals e and $\tilde{\eta}_2$ of the guidance system dynamics are bounded and practically prescribed-time stable.

Remark 9: The prescribed-time scaling function $\mu(t)$, where $\lim_{t \to t_0+T} \mu(t) = \infty$, is an analytical tool for ideal closed-loop convergence. In practice, however, unbounded gains near $t_0 + T$ are infeasible due to actuator, precision, and sampling limits. Hence, the gain is saturated as $\mu_s(t) = \min\{\mu(t), \mu_{\max}\}$, with $\mu_{\max} > 0$ chosen per hardware capabilities. This renders the implemented controller distinct from its ideal counterpart, replacing prescribed-time convergence with practical convergence to a residual neighborhood that shrinks as $\mu_{\max}$ grows. In simulations and experiments, $\mu_{\max} = 25$ balanced numerical robustness, actuation limits, and transient performance, with residual errors negligible relative to model uncertainties and noise. Such saturated implementations are also common in adaptive estimation frameworks under constraints [20].

Remark 10: The proposed prescribed-time framework fundamentally differs from conventional exponentially convergent adaptive and tracking schemes. For an exponentially stable system, the convergence rate is determined by the controller gains, and the time required for the tracking or estimation error to enter a prescribed neighborhood of the origin generally depends on the initial conditions. Specifically, if $\|e(t)\| \leq Ce^{-\lambda t}\|e(0)\|$, then the settling time satisfies $t \geq \frac{1}{\lambda} \ln(\frac{C\|e(0)\|}{\varepsilon})$, which explicitly depends on the initial error magnitude. Consequently, selecting controller gains alone cannot guarantee convergence within a predefined time for arbitrary initial conditions. In contrast, the proposed PT-LS/PT-LOS framework guarantees that both the parameter estimation and trajectory tracking errors converge within a user-specified prescribed time T_p, independently of the initial conditions, provided that the assumptions of Lemma 6 and Theorem 1 hold. This feature provides deterministic transient performance, which is particularly desirable for time-critical autonomous marine missions requiring guaranteed completion within predefined operational deadlines.

Proof: To prove Theorem 1, we first start by the kinematic closed-loop dynamics (57), which can be written in the form of the cascaded form (21) as $\dot{e} = f(t, e, \mu(t)) + g(t, e, \mu(t), \tilde{\eta}_2)$, where $f(t, e, \mu(t)) = -K_p \mu(t) e + \dot{\psi}_p S^T e - U \left[\frac{e_x}{\sqrt{\Delta^2(t) + e_x^2}}, \frac{e_y}{\sqrt{\Delta^2(t) + e_y^2}} \right]^\top$ and $g(t, e, \mu(t), \tilde{\eta}_2) = R_p(s)^\top \tilde{\eta}_2$. The Lyapunov function $V_{\text{kin}} = \frac{1}{2} e^\top e$ associated with (57), satisfies condition A) of Lemma 2, in fact, we have $\underline{\alpha}(\mu) =$

$\bar{\alpha}(\mu) = \frac{1}{2}$, furthermore, since $\mu(t) \geq 1$ for all $t \in [t_0, t_0 + T)$ and $m \geq 2$, we have $\frac{m+1}{m} = 1 + \frac{1}{m} > 1$. Hence $\|\boldsymbol{e}\| = 1 \cdot \|\boldsymbol{e}\| \leq \mu(t)^{\frac{m+1}{m}} \|\boldsymbol{e}\|$. Moreover, the time derivative of V_{kin} along the solutions of $\dot{\boldsymbol{e}} = \boldsymbol{f}(t, \boldsymbol{e}, \mu(t))$, results in $\frac{\partial V}{\partial e}\boldsymbol{f} \leq -2\lambda_{\min}(K_p)\mu(t)V$. Now $\mu(t) = \mu^{\frac{1}{m}}(t) \cdot \mu^{1-\frac{1}{m}}(t)$. However, we need a factor $\mu^{\frac{1}{m}}(t)$. For t sufficiently close to $t_0 + T$, $\mu(t)$ is large and $\mu^{1-\frac{1}{m}}(t) \geq 1$. Hence, $\mu(t) \geq \mu^{\frac{1}{m}}(t)$ for $\mu(t) \geq 1$. Thus, $\frac{\partial V}{\partial e}\boldsymbol{f} \leq -2\lambda_{\min}(K_p)\mu^{\frac{1}{m}}(t)V$. It is easy to verify that the perturbation term satisfies $\|\boldsymbol{g}(t, \boldsymbol{e}, \mu(t), \tilde{\boldsymbol{\eta}}_2)\| = \|\boldsymbol{R}_p(s)^\top \tilde{\boldsymbol{v}}_e\| \leq \|\tilde{\boldsymbol{v}}_e\|$. Therefore condition B) of lemma 2 is verified.

To show condition C) of lemma 2 also holds. Consider the transformed dynamics (58), along with the control input (59). Define the Lyapunov function $V_z = \frac{1}{2}\boldsymbol{z}^\top \boldsymbol{z} + \frac{1}{2}\tilde{\chi}^2$. From lemma 3 and lemma 4, it can be easily seen that $\mu(t)\boldsymbol{z}^\top \mathbf{u}_{\text{PT}} \leq -\mu(t)k\|\boldsymbol{z}\|^2 + \sqrt{\varepsilon}$ and $\mu(t)\boldsymbol{z}^\top \boldsymbol{d}_\eta \leq \mu(t)\chi\|\boldsymbol{z}\|\|\tanh(\frac{\mu(t)\boldsymbol{z}}{c_0})\| + \chi n c_0$, with $n = 2$. Applying the Young's inequality on the term $\mu(t)c_0\tilde{\chi}\hat{\chi}$, it can be obtained that $\mu(t)c_0\tilde{\chi}\hat{\chi} \leq \frac{\mu(t)c_0}{2}\chi^2 - \frac{\mu(t)c_0}{2}\tilde{\chi}^2$. Using these bounds to derive an upper bound for $\dot{V}_z$, yields

$$\begin{aligned}\dot{V}_z \leq\ & -\mu(t)k\|\boldsymbol{z}\|^2 + \sqrt{\varepsilon} + \mu(t)\|\boldsymbol{z}\|\|\mathbf{Y}^*\|\|\tilde{\boldsymbol{\Theta}}\| \\ & + \mu(t)\chi\|\boldsymbol{z}\|\left\|\tanh\left(\frac{\mu(t)\boldsymbol{z}}{c_0}\right)\right\| + \chi n c_0 \\ & - \mu(t)\tilde{\chi}\boldsymbol{z}^\top \tanh\left(\frac{\mu(t)\boldsymbol{z}}{c_0}\right) + \frac{\mu(t)c_0}{2}\chi^2 - \frac{\mu(t)c_0}{2}\tilde{\chi}^2.\end{aligned} \tag{61}$$

Note that $\mu(t)\chi\|\boldsymbol{z}\|\|\tanh(\cdot)\| - \mu(t)\tilde{\chi}\boldsymbol{z}^\top \tanh(\cdot) \leq \mu(t)\chi\|\boldsymbol{z}\|\|\tanh(\cdot)\| + \mu(t)|\tilde{\chi}|\|\boldsymbol{z}\|\|\tanh(\cdot)\|$, also by applying the Young's inequality one can obtain $\mu(t)|\tilde{\chi}|\|\boldsymbol{z}\|\|\tanh(\cdot)\| \leq \frac{\mu(t)}{2}\|\boldsymbol{z}\|^2\|\tanh(\cdot)\|^2 + \frac{\mu(t)}{2}\tilde{\chi}^2$. Observing also that $\mu(t)\chi\|\boldsymbol{z}\|\|\tanh(\cdot)\| \leq \mu(t)\chi\|\boldsymbol{z}\|$ since $\|\tanh(\cdot)\| \leq 1$, it implies by Young's inequality that $\mu(t)\chi\|\boldsymbol{z}\| \leq \frac{\mu(t)}{2}\|\boldsymbol{z}\|^2 + \frac{\mu(t)}{2}\chi^2$, the resulting inequality for $\dot{V}_z$ reduces to

$$\begin{aligned}\dot{V} \leq\ & -\mu(t)(k-1)\|\boldsymbol{z}\|^2 - \frac{\mu(t)}{2}(c_0 - 1)\tilde{\chi}^2 + \sqrt{\varepsilon} + \chi n c_0 \\ & + \mu(t)\|\boldsymbol{z}\|\|\mathbf{Y}^*\|\|\tilde{\boldsymbol{\Theta}}\| + \frac{\mu(t)}{2}(1 + c_0)\chi^2.\end{aligned} \tag{62}$$

Now for t sufficiently close to $t_0 + T$, $\|\tilde{\boldsymbol{\Theta}}\|$ is very small. Using Young's inequality, it is obtained that $\mu(t)\|\boldsymbol{z}\|\|\mathbf{Y}^*\|\|\tilde{\boldsymbol{\Theta}}\| \leq \frac{\mu(t)(k-1)}{2}\|\boldsymbol{z}\|^2 + \frac{\mu(t)}{2(k-1)}\|\mathbf{Y}^*\|^2\|\tilde{\boldsymbol{\Theta}}\|^2$, this yields $\dot{V}_z \leq -\frac{\mu(t)(k-1)}{2}\|\boldsymbol{z}\|^2 - \frac{\mu(t)}{2}(c_0 - 1)\tilde{\chi}^2 + \delta(t)$ where $\delta(t)$ is a bounded term given by $\delta(t) = \sqrt{\varepsilon} + \chi n c_0 + \frac{\mu(t)}{2(k-1)}\|\mathbf{Y}^*\|^2\|\tilde{\boldsymbol{\Theta}}\|^2 + \frac{\mu(t)}{2}(1 + c_0)\chi^2$, which can be written as $\dot{V}_z \leq -\gamma\mu(t)V_z + \delta$ where $\gamma = \min\{\frac{k-1}{2}, \frac{c_0-1}{2}\}$. Therefore, by lemma 1 the tracking errors $\boldsymbol{z}$ and $\tilde{\chi}$ are practical prescribed-time stable. It implies the tracking error $\tilde{\boldsymbol{\eta}}_2$ is practical prescribed-time stable.

To verify condition D), we identify from the cascade analysis that $\bar{\alpha}_s(\mu) = c_1\mu^{\frac{1}{m}}$, with $c_1 = 2\lambda_{\min}(K_p)$ and the interconnection gain: $\sigma_s(\mu) = \frac{1}{\bar{\alpha}_s(\mu)} = \frac{1}{c_1}\mu^{-\frac{1}{m}}$, we, therefore, have $\frac{d\sigma_s(\mu)}{d\mu} = -\frac{1}{c_1 m}\mu^{-1-\frac{1}{m}} \leq \frac{1}{c_1 m}\mu^{-1-\frac{1}{m}} = \frac{1}{2m}\mu^{-1-\frac{1}{m}}\sigma_s(\mu)\bar{\alpha}_s(\mu)$. Since $\sigma_s(\mu)\bar{\alpha}_s(\mu) = 1$ and $\frac{1}{c_1 m} = \frac{1}{2m} \cdot \frac{2}{c_1}$. The inequality holds because the left-hand side is negative while the right-hand side is positive. Then, for any $c_2 > 0$, the following hold $\frac{\sigma_s(\mu)c_2^2}{\exp(c_1)\bar{\alpha}_s(\mu)} < \infty$ for all $\mu \in [1, \infty)$. Condition D) of Lemma 2 is therefore satisfied.

All conditions have been verified, as a conclusion all tracking errors are practical prescribed-time convergent. □

Corollary 1: Consider the cascaded closed-loop system of Theorem 1, with the prescribed-time scaling function implemented as $\mu_s(t) = \min\{\mu(t), \mu_{\max}\}$, $\mu_{\max} > 1$. Suppose that the assumptions of Lemma 2 remain satisfied for all $\mu_s(t) \in [1, \mu_{\max}]$, and that the lower subsystem is uniformly ultimately bounded under the saturated implementation. Then, the complete cascaded system remains uniformly ultimately bounded. Moreover, the guidance error $\boldsymbol{e}$ and the velocity error $\tilde{\boldsymbol{\eta}}_2$ converge to a compact residual set whose size decreases as $\mu_{\max}$ increases. Therefore, gain saturation preserves the practical stability of the cascade while replacing the ideal prescribed-time convergence by practical convergence.

Proof: Since $\mu_s(t)$ is bounded, Conditions A)–D) of Lemma 2 remain valid on the compact interval $[1, \mu_{\max}]$. Furthermore, the lower subsystem is uniformly ultimately bounded, while the upper kinematic subsystem is ISS with respect to $\tilde{\boldsymbol{\eta}}_2$. Therefore, by the cascade stability result of Lemma 2, all closed-loop signals remain bounded and converge to a compact residual set. The radius of this set decreases as $\mu_{\max}$ increases, completing the proof. □

The overall experimental workflow sketching the proposed control approach implementation is given in Fig. 2.

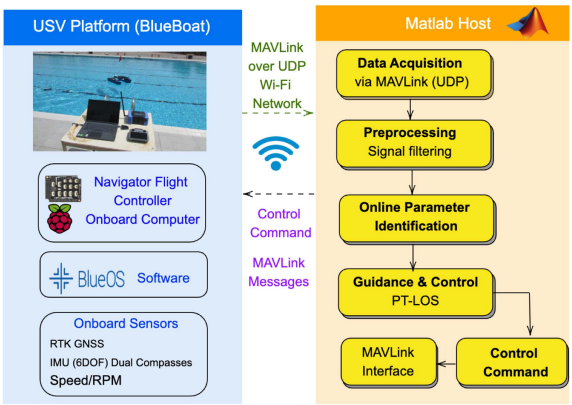

FIGURE 2. Real-time DREM-PT-LS identification and PT-LOS control architecture for the blackBoat USV.

V. EXPERIMENTAL VALIDATION

This section presents the experimental validation of the proposed approach. The experimental setup is first described, followed by the implementation of the PT-parameter estimation and PT-LOS guidance algorithm. Their control performance is then compared and assessed.

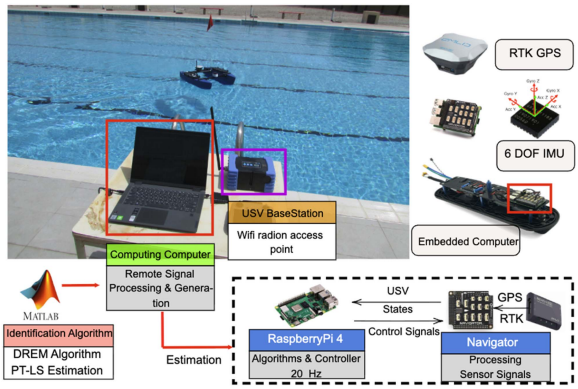

FIGURE 3. Physical experiment platform.

A. EXPERIMENTAL PLATFORM

The USV platform shown in Fig. 3 is a dual-hull catamaran design with a folding frame, measuring 1.20 m in length, 0.93 m in width, and 0.46 m in height when deployed. The propulsion system consists of two M200 motors driving weedless propellers, providing differential thrust for steering. The experimental platform consists of a black Robotics blackBoat equipped with a Navigator flight controller running ArduRover 4.6.0 firmware and a Raspberry Pi 4B onboard computer. The USV integrates RTK-GNSS, IMU, dual compasses, and propulsion feedback sensors for navigation and state measurement. Communication between the USV and the ground station is established through a shared 2.4 GHz Wi-Fi network using MAVLink-over-UDP telemetry. In the proposed architecture, MATLAB R2024b serves as the main real-time computation environment. Sensor measurements and vehicle states are transmitted from the blackBoat to the MATLAB host via MAVLink, where preprocessing, DREM-based composite parameter identification, PT-LS estimation, and PT-LOS guidance and control are executed online simultaneously. The computed surge and yaw commands are then sent back to the blackBoat as MAVLink messages, while the Navigator flight controller handles low-level actuation and motor execution. The proposed DREM-PT-LS identification and prescribed-time LOS control algorithms were executed at a fixed sampling frequency of 20 Hz within MATLAB. The prescribed-time horizon was selected sufficiently larger than the sampling interval to avoid excessively fast transients and numerical sensitivity near the terminal time. Moreover, to avoid excessively large adaptive gains and control amplitudes associated with the blow-up function $\mu(t)$ near $t = t_0 + T$, a bounded realization of the prescribed-time gain was employed using $\mu_s(t) = \min\{\mu(t), \mu_{\max}\}$, where $\mu_{\max} = 25$ was selected according to actuator, communication, and numerical limitations of the experimental platform.

The blackRobotics blackBoat[1] is used to instantiate the general 3-DOF dynamics from (1) with its physical specifications and estimated hydrodynamic coefficients. The vessel has a mass of $m = 14.5$ kg, a yaw moment of inertia $I_z = 5.0\ \text{kg} \cdot \text{m}^2$, and its center of gravity located at the body origin ($x_g = 0$). These parameters determine the inertia matrix M_i, which also accounts for added mass derivatives. Surge damping is modeled with both linear and quadratic terms, whereas sway and yaw damping include coupled nonlinear effects that depend on $|v|$ and $|r|$. Table 1 summarizes the complete set of numerical values, representing the nominal parameters used in the experiments.

TABLE 1. Blackboat Dynamic Model Parameters

Symbol	Description	Value
m	Mass	14.5 kg
I_z	Yaw inertia	5.0 kg·m^2
ε	virtual-point offset	0.45 m
Added Mass		
$X_{\dot{u}}$	Surge	−5.0 kg
$Y_{\dot{v}}$	Sway	−15.0 kg
$Y_{\dot{r}}$	Sway–yaw	−2.0 kg·m
$N_{\dot{r}}$	Yaw inertia	−2.0 kg·m^2
Damping		
X_u	Linear surge	−5.0 N s/m
$X_{\|u\|u}$	Quadratic surge	−10.0 N s^2/m^2
Y_v	Linear sway	−15.0 N s/m
$Y_{\|v\|v}$	Quadratic sway	−20.0 N s^2/m^2
Y_r	Sway–yaw	−0.5 N s
$Y_{\|r\|r}$	Quad yaw→sway	−1.0 N s^2
$Y_{\|v\|r}$	Cross	−0.5 N s^2/m
N_v	Sway–yaw	−0.5 N·m·s/m
$N_{\|v\|v}$	Quad sway–yaw	−1.0 N·m·s^2/m^2
N_r	Linear yaw	−2.0 N·m·s
$N_{\|r\|r}$	Quad yaw	−3.0 N·m·s^2
$N_{\|v\|r}$	Cross	−1.0 N·m·s^2/m

B. EXPERIMENTAL RESULTS AND ANALYSIS

At the start of the simulation ($t = 0$), the USV is positioned at coordinates ($x = 0$ m, $y = 0$ m) with an initial heading angle $\psi = 80^\circ$. The vessel has an initial surge velocity $u = 0.1$ m/s, while its sway velocity v and yaw rate r are both zero. The USV is tasked with following a closed-loop parametric path defined by the following equations:

$$x_d(s) = \frac{a\cos(s)}{1+\sin^2(s)},\ y_d(s) = \frac{a\sin(s)\cos(s)}{1+\sin^2(s)} \tag{63}$$

where $a = 8$ is a scaling parameter and $s \in [0, 2\pi]$ is the path parameter. This parametric curve produces a lemniscate path that the vessel must track (see Fig. 4). In the experiments, the IE condition was naturally satisfied through the lemniscate trajectory-following task. The repeated turning motions and coupled surge–yaw velocity variations generated sufficiently rich transient dynamics, resulting in a nonzero normalized excitation measure $\Phi_i(t) = \int_{t_0}^{t} \frac{\lambda_i^2(s)}{1+\mu^2(s)\lambda_i^2(s)}\,ds$ over a finite interval. Consequently, the required IE condition was satisfied without requiring PE. The controller architecture employs a LOS guidance law combined with separate speed and heading controllers. The LOS guidance computes the desired heading based on the cross-track error relative to the reference path. The LOS guidance parameters include the prescribed-time

[1][Online]. Available: https://blackrobotics.com/store/boat/blackboat/blackboat/

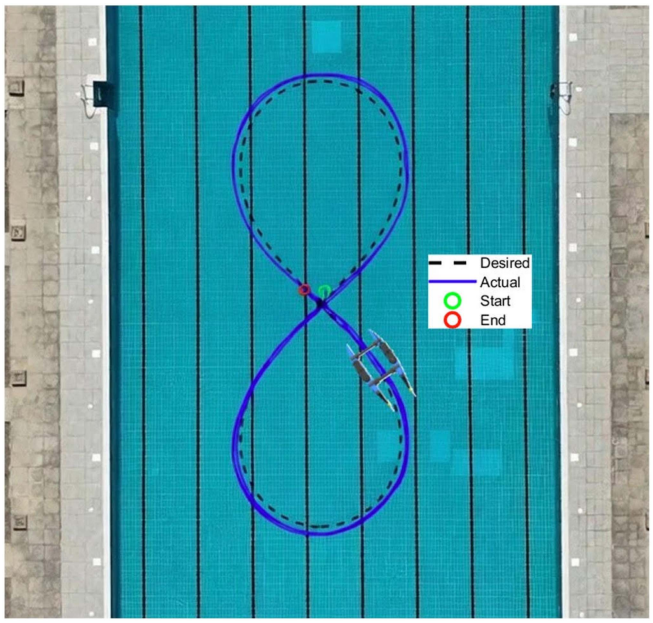

FIGURE 4. Actual path of the USV driven by the proposed method.

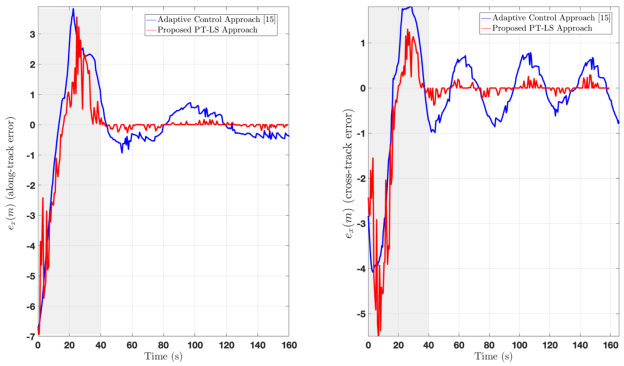

FIGURE 5. Path following tracking errors, the cross-track, and the along-track errors. Baseline adaptive control versus proposed PT-LS method in [15].

gain $K_p = 0.9I_2$ and the dynamic look-ahead distance Δ with initial look-ahead distance $\Delta_0 = 3.5$. The speed controller utilizes a surge speed gain $K_s = 0.9I_2$. The torque input control gain is $k_T = 9.3$. The disturbance compensator gain $\bar{c}_0 = 5.6$. The prescribed-time $T_p' = 40$ s. The speed reference is set to be $U_{\max} = 1.5$ m/s.

The proposed PT-LS approach was compared against baseline adaptive control algorithm [15] under identical initial conditions. Figs. 4–8 show the experiment results. Fig. 4 depicts the actual motion path of the USV using the proposed PT-LOS control method. The along-track and cross-track errors, e_x and e_y, converge to a small neighborhood of zero within the predefined time $T_p = 40$ s as shown in Fig. 5, where the proposed PT-LS approach is compared against baseline adaptive control algorithm [15] under identical initial conditions, demonstrating superior tracking accuracy with significantly reduced steady-state drift. The velocity tracking

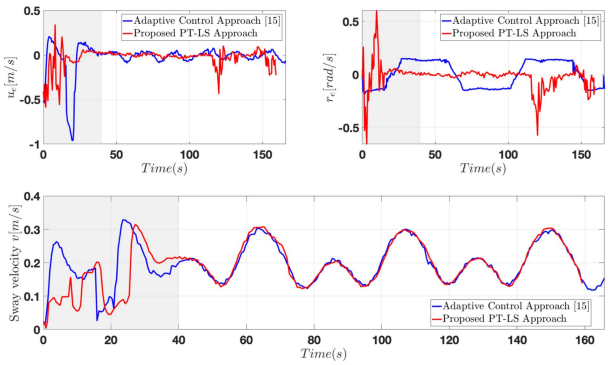

FIGURE 6. Velocity and angular velocity tracking errors.

error profiles shown in Fig. 6 further support this behavior, in which it is shown that the yaw rate error r_e decays rapidly and remains within ± 0.1 rad/s after the prescribed time $T_p = 40$ s, demonstrating effective rotational velocity regulation. The sway velocity error v_e also converges to a bounded values; however, sustained oscillations of approximately ± 0.3 m/s persist due to the continuously varying path curvature of the lemniscate trajectory and the absence of direct sway actuation. These oscillations are inherent to underactuated USV dynamics when following curved paths. Nevertheless, the magnitude of v_e remains within acceptable bounds and does not adversely affect the overall path-following accuracy. In compassion to [15], the proposed PT-LS approach achieves superior tracking performance compared to the adaptive control method, with the surge velocity error u_e and yaw rate error r_e converging more rapidly and maintaining higher precision throughout the trajectory. Meanwhile, the sway velocity error matches the adaptive control method [15], demonstrating comparable lateral velocity regulation. These results confirm that the PT-LS approach not only preserves the adaptive method's strengths in sway compensation but also enhances longitudinal and rotational velocity tracking accuracy.

The presented results in Fig. 7 demonstrate that the proposed DREM with PT-LS algorithm achieves globally consistent and practically prescribed-time convergence, while revealing important insights regarding parameter identifiability and excitation richness. Specifically, the first group of parameters θ_1–θ_5 converges rapidly within the initial few seconds, exhibiting smooth and nearly monotonic behavior with negligible oscillations. This indicates that the corresponding regressors are sufficiently rich and well-conditioned, enabling fast and accurate identification. In contrast, the second group of parameters θ_6–θ_{14}, exhibit transient oscillations and overshoot. This behavior can be attributed to weaker excitation, higher correlation among regressors, and interaction effects introduced at the stage transition. Nevertheless, ultimately all parameters converge to their true values before the prescribed-time $T_p = 40$ s, as clearly confirmed by the evolution of the norm $\|\tilde{\Theta}(t)\|$, which decreases to a neighborhood of zero at T_p and remains bounded thereafter without noticeable drift. This observation indicates that, although individual

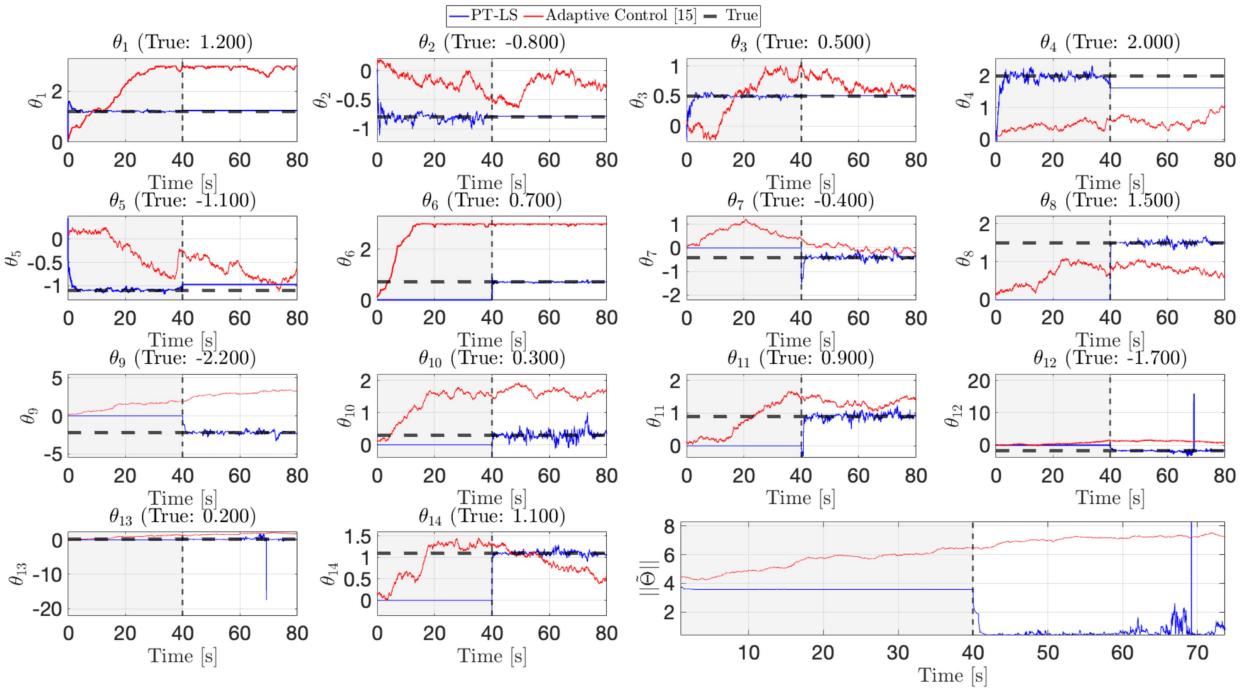

FIGURE 7. **Parameter estimations.**

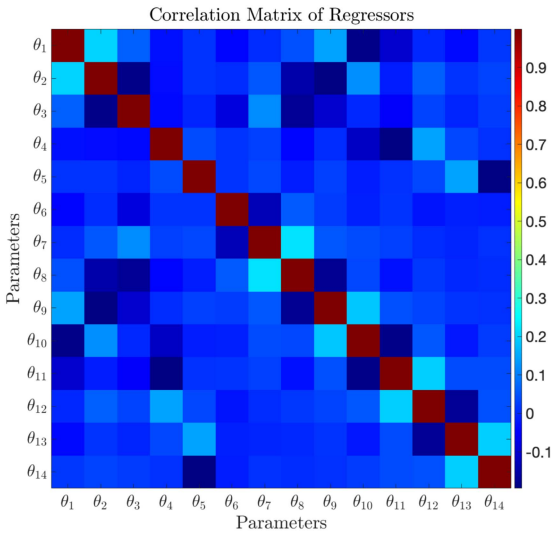

FIGURE 8. **Correlation matrix.**

parameters do not converge uniformly, the estimator guaranties global convergence within the prescribed-time horizon, which corroborates the results of Lemma 6, while also highlights the critical role of excitation quality and regressor conditioning in achieving uniform parameter-wise convergence.

The correlation matrix in Fig. 8 provides insight into the observed parameter convergence behavior. While most regressors exhibit low correlation, explaining the fast convergence of θ_1–θ_5, moderate correlation clusters appear among parameters θ_6–θ_{14}, particularly between (θ_7, θ_8), (θ_9, θ_{10}), and θ_{12}–θ_{14}. These partial linear dependencies reduce the effective excitation available for individual parameter identification, leading to transient oscillations and slower convergence near the prescribed time T_p. Nevertheless, the absence of strong correlations confirms that the regression model remains sufficiently informative to ensure convergence of all parameters within the prescribed-time horizon.

For comparison purposes, the proposed DREM with PT-LS framework is benchmarked against the Adaptive iLOS control method of [15] under identical noisy operating conditions. The results show that the proposed approach achieves significantly smaller parameter estimation errors and improved robustness. To quantitatively evaluate both methods, a composite cost index $J = w_1\bar{J}_{\text{ss}} + w_2\bar{J}_{\text{final}} + w_3\bar{J}_{\text{IAE}} + w_4\bar{J}_{\text{post}} + w_5\bar{J}_{\text{fluct}} + w_6\bar{J}_{\text{conv}}$ is introduced by combining several normalized performance metrics, including the steady-state mean parameter error, final parameter estimation error, integral absolute parameter estimation error (IAE), post-transient IAE, steady-state fluctuation, and convergence-time index, where $\bar{J}_i = \frac{J_i}{\max(J_i^{(\text{PTLS})}, J_i^{(\text{Adaptive})})}$ and the weighting coefficients satisfy $\sum_{i=1}^{6} w_i = 1$, $w_i > 0$. Smaller values of J indicate better overall estimation performance., where smaller values indicate better overall performance. In addition, a composite score is defined as Score $= 100(1 - J)$, such that larger scores correspond to superior performance. The proposed DREM with PT-LS method achieves $J = 0.2620$ and a score of 73.80/100, whereas the adaptive control approach yields $J = 0.9025$ and a score of only 9.75/100, confirming the superior estimation capability and robustness of the proposed framework. The IE condition was verified online by monitoring the normalized

TABLE 2. Comprehensive Comparison Index Between PT-LS and Adaptive iLOS Control in [15]

Metric	PT-LS	Adaptive Control in [15]
Steady-state mean parameter error	0.939150	7.290461
Final parameter error	0.323920	7.247424
IAE parameter error	2.119417	6.548508
Post-T_p IAE parameter error	0.652671	7.175631
Steady-state fluctuation	3.546381	0.090149
Convergence time index [s]	80.00	79.89
Composite cost J (lower is better)	0.2620	0.9025
Composite score (higher is better)	73.80/100	9.75/100
Excitation interval $[t_0, t^*]$ [s]	[0, 35]	N/A
Minimum normalized excitation level $\Phi^*_{\min} = \min_{i=1,\ldots,14} \Phi_i(t_e)$	0.78	N/A

excitation measure $\Phi_i(t)$ for each DREM channel. The excitation threshold was selected from a preliminary calibration run as $\epsilon_i = \rho\, \bar{\Phi}_i$, $\bar{\Phi}_i = \int_{t_0}^{t_e} \frac{\lambda_i^2(s)}{1+\mu^2(s)\lambda_i^2(s)}\, ds$, $0 < \rho < 1$ where ρ is a prescribed design constant. The excitation completion time t^* was then defined as the first instant at which $\Phi_i(t) \geq \epsilon_i$, $\forall i = 1, \ldots, 14$. In addition, Table 2 shows that the proposed lemniscate maneuver satisfied this condition within the first 35 s of operation. Consequently, sufficient excitation was accumulated during this finite interval to guarantee the prescribed-time convergence of the PT-LS estimator, without requiring the PE condition thereafter.

VI. CONCLUSION

This work proposed a composite parameter estimation approach combining DREM with a PT-LS adaptation law to address unknown model uncertainties. The method estimates composite parameters capturing the overall system dynamics, which achieve practical convergence within the prescribed time $T_p = 40$ s. Based on these estimates, a PT-LOS controller was developed, enabling accurate path-following within the same predefined time horizon. Numerical and experimental results confirm that the proposed strategy significantly reduces path-following errors and achieves faster convergence and improved tracking accuracy compared to the reference approach, demonstrating strong robustness against model uncertainties and disturbances. Future work will explore artificial intelligence techniques to compensate for bias drift and unmodeled dynamics.

APPENDIX A

Proof of Lemma 2

The proof follows the changing Lyapunov function method as in [48] and consists of defining a scaled Lyapunov function: $W(\mu, x) = \sigma_s(\mu)V(\mu, x)$, with $\sigma_s(\mu)$ is a continuously differentiable function of class $\mathcal{K}_\infty$ satisfying $\frac{d\sigma_s(\mu)}{d\mu} \leq \frac{1}{2m}\mu^{-1-\frac{1}{m}}\sigma_s(\mu)\bar{\alpha}_s(\mu)$. Using Conditions A0 and B), the time differentiation of $W(\mu, x)$ leads to

$$\dot{W} \leq \frac{d\sigma_s}{d\mu}\frac{m}{T}\mu^{1+\frac{1}{m}}V - c_1\mu^{\frac{1}{m}}\sigma_s V + \sigma_s\mu^{\frac{m+1}{m}}\|x\|c_2\|\xi_e\|. \tag{64}$$

Applying condition (26) to bound $\frac{d\sigma_s}{d\mu}\dot{\mu}$, results in $\frac{d\sigma_s}{d\mu}\dot{\mu}V \leq\leq \frac{1}{2m}\mu^{-1-\frac{1}{m}}\sigma_s\bar{\alpha}_s \cdot \frac{m}{T}\mu^{1+\frac{1}{m}}V = \frac{1}{2T}\bar{\alpha}_s\sigma_s V$, which when substituted in (64), yields $\dot{W} \leq (\frac{1}{2T}\bar{\alpha}_s - c_1\mu^{\frac{1}{m}})\sigma_s V + c_2\sigma_s\mu^{\frac{m+1}{m}}\|x\|\|\xi_e\|$. Since $\bar{\alpha}_s(\mu)$ is a prescribed-time convergent gain and $c_1 > 2$, we can choose $\bar{\alpha}_s(\mu) \leq 2Tc_1\mu^{1/m}$ for sufficiently large μ, which gives $\frac{1}{2T}\bar{\alpha}_s - c_1\mu^{1/m} \leq -\frac{c_1}{2}\mu^{1/m}$. Thus

$$\dot{W} \leq -\frac{c_1}{2}\mu^{\frac{1}{m}}W + c_2\sigma_s\mu^{\frac{m+1}{m}}\|x\|\|\xi_e\|. \tag{65}$$

Using Young's inequality on the last term of (65), and using the fact that $\bar{\alpha}_s \leq 2Tc_1\mu^{1/m}$, it is obtained that $c_2\sigma_s\mu^{\frac{m+1}{m}}\|x\|\|\xi_e\| \leq \frac{c_1}{2}\mu^{\frac{1}{m}}W + \frac{1}{2}\sigma_s\mu^{\frac{2m+1}{m}}c_2^2\|\xi_e\|^2$. It can be inferred that $\dot{W} \leq \frac{1}{2}\sigma_s\mu^{\frac{2m+1}{m}}c_2^2\|\xi_e\|^2$. By condition (27), there exists a constant $M > 0$ such that $\sigma_s(\mu)c_2^2 \leq M\exp(c_1)\bar{\alpha}_s(\mu)$. Moreover, note that $\mu^{(2m+1)/m} \leq \bar{\alpha}_s(\mu)$ for sufficiently large μ (since $\bar{\alpha}_s$ is $\mathcal{K}_\infty$). Thus

$$\dot{W} \leq \frac{M}{2}\exp(c_1)\bar{\alpha}_s(\mu)\|\xi_e\|^2. \tag{66}$$

Now, define the integrating factor $\kappa(t)$ such that $\kappa(t) = \exp(\int_{t_0}^{t}\frac{c_1}{2}\mu(\tau)^{\frac{1}{m}}d\tau) = (1 - \frac{t-t_0}{T})^{-\frac{c_1 T}{2}}$. From (66), we obtain

$$\frac{d}{dt}(\kappa(t)W(t)) \leq \frac{M}{2}\exp(c_1)\bar{\alpha}_s(\mu)\kappa(t)\|\xi_e(t)\|^2. \tag{67}$$

Integrating (67) from t_0 to t and using the PPTS of ξ_e from condition C), for any given $\delta > 0$, it is obtained the following: $\kappa(t)W(t) \leq W(t_0) + M\exp(c_1)\int_{t_0}^{t}\bar{\alpha}_s(\mu(\tau))\kappa(\tau)\beta_\xi^2(\|\xi_e(t_0)\|, \tau - t_0)d\tau + M\exp(c_1)\delta^2\int_{t_0}^{t}\bar{\alpha}_s(\mu(\tau))\kappa(\tau)d\tau$. Notice also that $\int_{t_0}^{t}\bar{\alpha}_s(\mu(\tau))\kappa(\tau)d\tau$ is bounded for all $t \in \mathcal{T}_p$. Let $\Lambda = \sup_{t\in\mathcal{T}_p}\int_{t_0}^{t}\bar{\alpha}_s(\mu(\tau))\kappa(\tau)d\tau < \infty$. Furthermore, since $\beta_\xi \in \mathcal{KL}_T^e$, the term $\int_{t_0}^{t}\bar{\alpha}_s(\mu(\tau))\kappa(\tau)\beta_\xi^2(\|\xi_e(t_0)\|, \tau - t_0)d\tau$ remains bounded as $t \to t_0 + T$, and $\kappa^{-1}(t)$ multiplied by this integral tends to zero. Thus, we have $W(t) \leq \varepsilon + M\exp(c_1)\delta^2\kappa^{-1}(t)\Lambda$. Using the lower bound $V \geq \underline{\alpha}(\mu)\|x\|^2$ and the fact that $\kappa^{-1}(t) \leq 1$ for all $t \in \mathcal{T}_p$, we obtain

$$\|x(t)\| \leq \sqrt{\frac{\varepsilon}{\underline{\alpha}(\mu(t))}} + \sqrt{\frac{M\exp(c_1)\Lambda}{\underline{\alpha}(\mu(t))}}\delta. \tag{68}$$

Since $\underline{\alpha}(\mu(t))$ is bounded away from zero for finite $\mu(t)$, we can define $\epsilon = \sup_{t\in\mathcal{T}_p} \sqrt{\frac{M\exp(c_1)\Lambda}{\underline{\alpha}(\mu(t))}} < \infty$, it implies that $\|x(t)\| \leq \beta_x(\|x(t_0)\|, t-t_0) + \epsilon\delta + \sqrt{\frac{\varepsilon}{\underline{\alpha}(\mu(t))}}$ where β_x absorbs the transient terms. For sufficiently small δ, we can ensure $\epsilon\delta \leq \varepsilon$, yielding $\lim_{t\to t_0+T} \|x(t)\| \leq 2\varepsilon$. Since $\varepsilon > 0$ can be chosen arbitrarily small by taking δ sufficiently small and selecting t^* appropriately, we conclude that $x(t)$ converges to an arbitrarily small neighborhood of zero at the prescribed-time $t_0 + T$, i.e., PPTS is achieved.

REFERENCES

[1] J. Alberti, "Modeling and model identification of autonomous underwater vehicles," Master Sci. Mech. Eng. Naval Postgraduate Sch., Monterey, California, Rep. ADA1009363, 2015.

[2] V. Andrieu, L. Praly, and A. Astolfi, "Homogeneous approximation, recursive observer design, and output feedback," *SIAM J. Control Optim.*, vol. 47, no. 4, pp. 1814–1850, 2008.

[3] S. Aranovskiy, A. Bobtsov, R. Ortega, and A. Pyrkin, "Performance enhancement of parameter estimators via dynamic regressor extension and mixing," *IEEE Trans. Autom. Control*, vol. 62, no. 7, pp. 3546–3550, Jul. 2017.

[4] S. Aranovskiy, A. Bobtsov, R. Ortega, and A. Pyrkin, "Adaptive control of linear multivariable systems using dynamic regressor extension and mixing estimators: Removing the high-frequency gain assumptions," *Automatica*, vol. 110, 2019, Art. no. 108589.

[5] R. Beltran-Aguedo and M. A. Jordan, "A method for continuous-time identification of moored marine systems," *Latin Amer. Appl. Res.*, vol. 33, no. 4, pp. 333–340, 2003.

[6] A. Bobtsov, B. Yi, R. Ortega, and A. Astolfi, "Generation of new exciting regressors for consistent online estimation of unknown constant parameters," *IEEE Trans. Autom. Control*, vol. 67, no. 9, pp. 4746–4753, Sep. 2022.

[7] A. Boretti, "Navigating the future: The expanding role of unmanned surface vehicles in maritime security," *J. Transp. Secur.*, vol. 18. no. 24, pp. 1–23, 2025.

[8] E. Cruz-Zavala, J. Moreno, and L. Fridman, "Uniform robust exact differentiator," *IEEE Trans. Autom. Control*, vol. 56, no. 11, pp. 2727–2733, Nov. 2011.

[9] Y. Deng, Z. Zhang, M. Gong, and T. Ni, "Event-triggered asymptotic tracking control of underactuated ships with prescribed performance," *IEEE Trans. Intell. Transp. Syst.*, vol. 24, no. 1, pp. 645–656, Jan. 2023.

[10] Z. Dong, Y. Ding, W. Liu, Z. Hu, S. Lu, and Y. Liu, "Maneuverability parameter identification of a water-jet USV based on truncated weighted LSSVM integrated with adaptive mutation PSO algorithm," *Ocean Eng.*, vol. 321, 2025, Art. no. 120474.

[11] Z. Du, Y. Yang, J. Zhu, and Y. Lyu, "Online parameter estimation for fixed-wing UAV based on DREM method and adaptive control," *IEEE Trans. Aerosp. Electron. Syst.*, vol. 61, no. 2, pp. 1363–1376, Apr. 2025.

[12] D. Efimov and A. Fradkov, "Design of impulsive adaptive observers for improvement of persistency of excitation," *Int. J. Adaptive Control Signal Process.*, vol. 29, no. 6, pp. 765–782, 2015.

[13] G. Fontenla-Carrera, E. Aldao Pensado, F. Veiga-López, and H. González-Jorge, "Efficient offshore wind farm inspections using a support vessel and UAVs," *Ocean Eng.*, vol. 332, 2025, Art. no. 121416.

[14] Thor. I. Fossen, *Marine Craft Hydrodynamics and Motion Control*. Hoboken, NJ, USA: Wiley, 2011.

[15] Thor I. Fossen and A. M. Lekkas, "Direct and indirect adaptive integral line-of-sight path-following controllers for marine craft exposed to ocean currents," *Int. J. Adaptive Control Signal Process.*, vol. 31, no. 4, pp. 445–463, 2017.

[16] J. Ghommam, M. Saad, M. H. Rahman, and Q. Zhu, "Prescribed performance resilient motion coordination with actor–critic reinforcement learning design for UAV-USV systems," *IEEE Trans. Artif. Intell.*, vol. 6, no. 12, pp. 3336–3350, Dec. 2025.

[17] A. Glushchenko and K. Lastochkin, "Instrumental variables based DREM for online asymptotic identification of perturbed linear systems," *IEEE Trans. Autom. Control*, vol. 70, no. 2, pp. 1320–1327, Feb. 2025.

[18] J. Holloway and M. Krstic, "Prescribed-time observers for linear systems in observer canonical form," *IEEE Trans. Autom. Control*, vol. 67, no. 11, pp. 6080–6087, Sep. 2022.

[19] M. Korotina, S. Aranovskiy, R. Ushirobira, D. Efimov, and J. Wang, "Fixed-time parameter estimation via the discrete-time DREM method," *IFAC-PapersOnLine*, vol. 56, no. 2, pp. 4013–4018, 2023.

[20] W. Li and M. Krstic, "Adaptive nonlinear prescribed-time control with filterless least squares," *IEEE Trans. Autom. Control*, vol. 70, no. 9, pp. 5880–5893, Sep. 2025.

[21] L. Liu, D. Wang, Z. Peng, and Q.-L. Han, "Distributed path following of multiple under-actuated autonomous surface vehicles based on data-driven neural predictors via integral concurrent learning," *IEEE Trans. Neural Netw. Learn. Syst.*, vol. 32, no. 12, pp. 5334–5344, Dec. 2021.

[22] Z. Lv, X. Wang, G. Wang, X. Xing, C. Lv, and F. Yu, "Unmanned surface vehicles in marine surveillance and management: Advances in communication, navigation, control, and data-driven research," *J. Mar. Sci. Eng.*, vol. 13, no. 5, pp. 969, 2025.

[23] J. P. Martinez-Esteso, F. J. Castellanos, J. Calvo-Zaragoza, and A. J. Gallego, "Maritime search and rescue missions with aerial images: A survey," *Comput. Sci. Rev.*, vol. 57, 2025, Art. no. 100736.

[24] J. Matouš, K. Y. Pettersen, D. Varagnolo, M. S. Rundhovde, and C. Paliotta, "Path following control of a towed marine system," *Control Eng. Pract.*, vol. 170, 2026, Art. no. 106845.

[25] R. Nair, L. Behera, and S. Kumar, "Event-triggered finite-time integral sliding mode controller for consensus-based formation of multirobot systems with disturbances," *IEEE Trans. Control Syst. Technol.*, vol. 27, no. 1, pp. 39–47, Jan. 2019.

[26] S. K. Narendra and A. M. Annaswamy, "Persistent excitation in adaptive systems," *Int. J. Control*, vol. 45, no. 1, pp. 127–160, 1987.

[27] D. E. Ochoa, N. Espitia, and J. I. Poveda, "Prescribed-time stability in switching systems with resets: A hybrid dynamical systems approach," *Syst. Control Lett.*, vol. 193, 2024, Art. no. 105910.

[28] R. Ortega, S. Aranovskiy, and A. Pyrkin, "Necessary and sufficient conditions for convergence of DREM-based estimators with applications in adaptive control," *Automatica*, vol. 146, 2022, Art. no. 110597.

[29] R. Ortega, V. Nikiforov, and D. Gerasimov, "On modified parameter estimators for identification and adaptive control. A unified framework and some new schemes," *Annu. Rev. Control*, vol. 50, pp. 278–293, 2020.

[30] Y. Pan, Meng Joo Er, Y. Liu, L. Pan, and H. Yu, "Composite learning fuzzy control of uncertain nonlinear systems," *Int. J. Fuzzy Syst.*, vol. 18, no. 6, pp. 990–998, 2016.

[31] Y. Pan, T. Sun, Y. Liu, and H. Yu, "Composite learning from adaptive backstepping neural network control," *Neural Netw.*, vol. 95, pp. 134–142, 2017.

[32] Y. Pan and H. Yu, "Composite learning from adaptive dynamic surface control," *IEEE Trans. Autom. Control*, vol. 61, no. 9, pp. 2603–2609, Sep. 2016.

[33] Z. Peng, Y. Jiang, L. Liu, and Y. Shi, "Path-guided model-free flocking control of unmanned surface vehicles based on concurrent learning extended state observers," *IEEE Trans. Syst., Man, Cybern. Syst.*, vol. 53, no. 8, pp. 4729–4739, Aug. 2023.

[34] Z. Peng, J. Wang, D. Wang, and Q.-L. Han, "An overview of recent advances in coordinated control of multiple autonomous surface vehicles," *IEEE Trans. Ind. Informat.*, vol. 17, no. 2, pp. 732–745, Feb. 2021.

[35] L. P. Perera, P. Oliveira, and C. G. Soares, "System identification of vessel steering with unstructured uncertainties by persistent excitation maneuvers," *IEEE J. Ocean. Eng.*, vol. 40, no. 2, pp. 456–467, Jul. 2016.

[36] A. Polyakov, "Nonlinear feedback design for fixed-time stabilization of linear control systems," *IEEE Trans. Autom. Control*, vol. 57, no. 8, pp. 2106–2110, Aug. 2012.

[37] A. C. Rencher and W. F. Christensen, *Methods of Multivariate Analysis* (Probability and Statistics), 3rd ed. Hoboken, NJ, USA: Wiley, 2012.

[38] Y. Song, Y. Wang, J. Holloway, and M. Krstić, "Time-varying feedback for regulation of normal-form nonlinear systems in prescribed finite time," *Automatica*, vol. 83, pp. 243–251, 2017.

[39] J. Wang, D. Efimov, S. Aranovskiy, and Alexey A. Bobtsov, "Fixed-time estimation of parameters for non-persistent excitation," *Eur. J. Control*, vol. 55, pp. 24–32, 2020.

[40] J. Wang, D. Efimov, and A. A. Bobtsov, "On robust parameter estimation in finite-time without persistence of excitation," *IEEE Trans. Autom. Control*, vol. 65, no. 4, pp. 1731–1738, Apr. 2020.

[41] Y. Wang, W. Liu, J. Liu, and C. Sun, "Cooperative USV–UAV marine search and rescue with visual navigation and reinforcement learning-based control," *ISA Trans.*, vol. 137, pp. 222–235, 2023.
[42] G. Wen, J. Fu, B. Wang, X. Wang, and H. Shen, "Robust formation tracking of ASVs with nonconservative collision avoidance: A control barrier function-based approach," *IEEE Trans. Ind. Electron.*, vol. 73, no. 6, pp. 9174–9186, Jun. 2026.
[43] X. Xiang, C. Yu, L. Lapierre, J. Zhang, and Q. Zhang, "Survey on fuzzy-logic-based guidance and control of marine surface vehicles and underwater vehicles," *Int. J. Fuzzy Syst.*, vol. 20, no. 2, pp. 572–586, Feb. 2018.
[44] X. Yan, *Linear Regression Analysis: Theory and Computing*. Singapore: World Scientific, 2009.
[45] Y. Yao, Y. Kang, Y. Zhao, P. Li, and J. Tan, "A novel prescribed-time control approach of state-constrained high-order nonlinear systems," *IEEE Trans. Syst., Man, Cybern. Syst.*, vol. 54, no. 5, pp. 2941–2951, May 2024.
[46] J. Yue, L. Liu, Z. Peng, D. Wang, and T. Li, "Data-driven adaptive extended state observer design for autonomous surface vehicles with unknown input gains based on concurrent learning," *Neurocomputing*, vol. 467, pp. 337–347, 2022.
[47] D. Zeng, C. Cai, Y. Liu, J. Zhao, and C. Li, "Practical prescribed-time control for underactuated marine surface vessels: Theory and experiment," *IEEE Trans. Autom. Sci. Eng.*, vol. 22, pp. 14074–14083, 2025.
[48] G. Zuo, L. Zhu, Y. Wang, Z. Chen, and Y. Song, "Achieving distributed convex optimization within prescribed time for high-order nonlinear multiagent systems," *IEEE Trans. Cybern.*, vol. 55, no. 10, pp. 4784–4797, Oct. 2025.